Energy Conversion and Management 358 (2026) 121457

Contents lists available at ScienceDirect

Energy Conversion and Management

journal homepage: www.elsevier.com/locate/enconman

Analysis of a novel nuclear electrothermal steam reforming scheme for clean industrial hydrogen

Rami S. El-Emam [a,b,*], Rahaf Ajaj [c,d], Khaoula Khlie [e], Calin Zamfirescu [f]

[a] Brilliant Energy Institute, Ontario Tech University, Oshawa, ON, Canada
[b] Faculty of Engineering, Mansoura University, Mansoura, Egypt
[c] College of Engineering, Abu Dhabi University, Abu Dhabi, United Arab Emirates
[d] Research Institute for Sustainable Futures, Abu Dhabi University, Abu Dhabi, United Arab Emirates
[e] Industrial Management Department, Liwa University, United Arab Emirates
[f] Faculty of Science and Engineering Technology, Durham College, Oshawa, ON, Canada

ARTICLE INFO

Keywords:
Nuclear hydrogen
Small nuclear reactor
Electrified steam methane reforming
Circulating fluidized bed reformer
Hydrogen-selective membrane
Direct carbon capture
Refinery decarbonization

ABSTRACT

This work develops and evaluates a nuclear electro-thermal steam methane reformer (SMR) architecture for refinery-scale hydrogen production in which a small modular nuclear reactor (SMNR) supplies steady steam and electricity. At the same time, the reforming duty is delivered electrically to a compact, responsive reformer. The SMR core is implemented as a circulating fluidized-bed reactor (CFBR) with cyclone separation and electrical reheating of recirculated catalyst in four heated diplegs, enabling near-isothermal operation and fast thermal response. Hydrogen is withdrawn via external Ni-based H_2-selective membranes (two modules sized for the main permeate and downstream polishing). In contrast, downstream conditioning is provided by high-temperature and low-temperature water–gas shift. Carbon management is achieved by confining carbon to the syngas/tail-gas loop and applying a compact oxidation/condensation approach to generate a concentrated CO_2 stream suitable for capture. Multiple Aspen Plus flowsheets coupled to an Engineering Equation Solver (EES) steam-Rankine model is used to synthesize the integrated process and quantify plant-level performance. At the design point, the plant produces ~113 t/day H_2 while capturing ~614 t/day CO_2, with an overall electricity demand of ~13.2 kWh per kg H_2, substantially below the ~55 kWh per kg H_2 typical of proton exchange membrane (PEM) electrolysis at similar output. The results indicate that nuclear electro-thermal steam methane reforming (NET-SMR) is an "electricity-light" pathway to low-carbon refinery hydrogen that preserves SMR's scale advantages while enabling high CO_2 capture and nuclear-compatible heat-power integration.

1. Introduction

Hydrogen is essential for petroleum refining, ammonia and methanol production, direct-reduced iron, and various chemical processes, with large facilities often consuming tens to hundreds of tonnes daily. Since the early 20th century, steam-methane reforming (SMR) has been the a dominant production method due to its lower energy requirements than water electrolysis. However, SMR is highly carbon-intensive, emitting 9–12 kg of CO_2 per kg of H_2 when accounting for both process and furnace emissions. Traditional SMR relies on fired tube reactors operating at 600–900°C and 10–30 bar, burning about one-third of the natural gas feed for heat. This design faces challenges such as large temperature gradients, coking risks, and slow thermal response times (on the order of weeks), which limit operational flexibility and hinder decarbonization efforts [1].

These inherent limitations have driven the emergence of electrified SMR (eSMR) as a transformative new approach, representing a significant technological advancement in hydrogen production. This new technology replaces fossil-fired heating with direct electrical energy (resistive, microwave, or induction), fundamentally changing the reforming paradigm if the electricity is sourced from nuclear or renewable sources. As a groundbreaking innovation, eSMR eliminates the furnace and its emissions while confining CO_2 to the syngas loop for easier capture. This cutting-edge approach achieves comparable conversion rates (75–95%) in dramatically smaller reactors (4–15 m^3 vs >1000 m^3), enables faster start-up (minutes-hours instead of days-weeks), and reaches superior efficiencies (up to 97.27% thermal and 88.68% electrical in optimized configurations), with projected hydrogen

* Corresponding author at: Ontario Tech University, Canada.
E-mail address: rami.elemam@ontariotechu.ca (R.S. El-Emam).

https://doi.org/10.1016/j.enconman.2026.121457
Received 7 January 2026; Received in revised form 3 April 2026; Accepted 5 April 2026
Available online 17 April 2026

costs of $2.5–3.4/kg under favorable electricity pricing, Refs. [1,2].

Electrified SMR utilizes three advanced electric heating methods, each with distinct advantages: Joule (resistive) heating offers near-perfect efficiency, precise control, and uniform thermal profiles in a compact design, refs. [1,3,4]; microwave heating enables direct volumetric energy coupling to dielectric/semiconductive media but requires optimized cavity designs; and induction heating provides wireless, localized heating through magnetic catalysts (e.g., Co-Ni susceptors) paired with radio-frequency coil systems.

Electrifying SMR is especially well-suited to packed-bed tubular reformers, where the catalyst is held in a porous bed inside a metallic tube; direct Joule heating or induction heating of the tube shortens the thermal path and improves heating efficiency. A potentially larger step-change, however, comes from integrating a hydrogen-selective membrane to remove H_2 in situ, shift the equilibrium, and raise conversion. To our knowledge, no practical design has been demonstrated in which the same tubular wall serves simultaneously as the resistive heater and as the H_2-selective membrane materials, and manufacturing constraints (electrical conductivity vs. selective permeability, embrittlement, and thermal-cycling durability) make this coupling impractical today. Motivated by these limits, this study investigates an alternative architecture: applying electric heating and membrane separation in a circulating fluidized-bed loop, decoupling heat addition from separation so each function can use optimal materials while retaining fast, uniform heating and high mass-transfer rates.

Although nuclear electricity could in principle be routed entirely to water electrolysis, a nuclear-electro-thermal SMR architecture exploits electricity and natural gas more synergistically for large refinery hydrogen units. In electrolysis, all of the hydrogen enthalpy must be supplied electrically by splitting water, leading to specific electricity consumptions of order 50–55 kWh/kg H_2 for typical alkaline/PEM systems. By contrast, in electro-thermal SMR, a large fraction of the hydrogen energy still comes from the chemical exergy of natural gas. At the same time, electricity is used only to provide high-grade heat and drive auxiliaries. As a result, the electrically heated reformer produces "blue" hydrogen with roughly an order of magnitude lower electricity demand per kilogram of H_2 than electrolysis, for similar CO_2 capture rates, so a given nuclear power block can decarbonize a much larger refinery hydrogen load. In this paper, "efficiency improvement" refers to reduced plant-gate specific electricity demand and, where stated, to exergy efficiency on the chosen hydrogen-plus-power cogeneration basis; it is not intended as a universal claim of superior primary-energy efficiency or full lifecycle efficiency.

Recent techno-economic and life-cycle benchmarking studies report low-temperature electrolysis alongside steam methane reforming (SMR) and autothermal reforming (ATR) with carbon capture and storage (CCS), i.e., conventional "blue hydrogen", on consistent cost and greenhouse gas (GHG) accounting. Therefore, the electrolysis comparator adopted here also provides a transparent bridge to the policy-relevant blue-hydrogen benchmark, such as those provided in Refs. [34–36]. The electrolysis-vs-blue benchmarking sources used for context represent "blue hydrogen" primarily as SMR with CCS. Reported capture performance is typically described as $>$ 90% of direct plant emissions for CCS-equipped reforming, with techno-economic analyses baselines reporting capture rates on the order of the mid-90% range.

The capital and integration logic are also different. Conventional SMR is already deployed at 100–1000 + t/day H_2, with well-understood reactors, catalysts, shift, and membrane/separation technology, at capital intensities on the order of 0.5–0.9 k$/(kg H_2/day). In contrast, electrolyzer plants are still about 2 times more capital-intensive, with ≈1–1.8 k$/(kg H_2/day), and must be from thousands of small cells and tens to hundreds of stacks, with kilometers of piping, complex manifolding, and periodic membrane replacement to achieve a comparable capacity with regular SMR plants. A 100+ t/day electrolyzer train requires on the order of 10,000 individual cells and 1–3 km of gas and water headers. In contrast, an electro-thermal SMR unit of the same capacity is realized in a single fluidized-bed reformer plus a few membrane and shift vessels.

For refinery hosts, electro-thermal SMR therefore offers a more natural near-term pathway: the existing natural-gas supply, pressure levels, and hydrogen distribution are preserved; compact electric heaters and nuclear-derived steam replace the fired furnace; and all carbon is confined to one or two concentrated CO_2 streams that can be captured at a high rate. This preserves the economies of scale and process familiarity of SMR while using nuclear heat and power to suppress furnace emissions, lower natural-gas consumption, and greatly reduces the electricity footprint per tonne of low-carbon hydrogen relative to an all-electrolysis configuration.

From a nuclear-energy application perspective, refinery and petrochemical sites are especially relevant hosts because they require both continuous hydrogen production and large, steady steam-and-power services. Small modular nuclear reactors (SMNRs) are therefore attractive not only as low-carbon electricity sources, but also as cogeneration systems that can supply process steam, feedwater heating, and electrical auxiliaries from a common balance of plant. This coupling is technically important because it aligns the high-capacity-factor operation of nuclear systems with the similarly continuous duty of refinery hydrogen units, while preserving existing natural-gas and hydrogen distribution infrastructure and reducing reliance on very large dedicated electrical supply for all-electrolysis Refs. [23,24,26,30].

This paper develops and evaluates nuclear electro-thermal steam reforming of natural gas (NET-SMR) for industrial hydrogen production on the order of 100 t/day. The concept is intended as a practical nuclear cogeneration application in which reactor output is used in forms that are already natural to industrial deployment – namely steam, feedwater heating, and electricity – rather than requiring the nuclear plant to serve only as an indirect electricity source for hydrogen production. Building on recent experience with electrically heated SMR (eSMR), we design a custom steam-Rankine power cycle that couples to the makeup-gas preheating loop, enabling seamless integration of a small modular nuclear reactor (SMNR) with the reformer. The reformer is implemented as a circulating fluidized-bed reactor (CFBR) with cyclone solids separation and resistive reheating of the recirculated particulate catalyst. Low-cost nickel-based membranes separate hydrogen from the product gas, while the retentate is partially recycled and sufficiently preheated before returning to the CFBR. Aspen Plus is used to synthesize the preheating, reaction, and separation trains and to co-optimize their integration with the nuclear-driven steam-Rankine cycle. Direct CO_2 capture is achieved through a compact oxy-fuel combustion system that fully oxidizes the unreacted combustible fraction in the exhaust stream. Oxygen is supplied by a low-capacity electrolyzer and metered near the stoichiometric requirement, allowing subsequent CO_2 removal primarily by stripping and water condensation. This configuration improves overall economics by achieving effective carbon capture with minimal additional process complexity.

2. Literature review

Prior work on low-carbon hydrogen from methane reforming clusters around three quantitative threads that directly inform the present model: (i) electrified SMR (eSMR), which replaces fired radiant duty with electrical heating and establishes realistic operating windows and efficiencies; (ii) membrane-assisted reforming, which uses selective H_2 withdrawal (Pd- or Ni-based) to shift equilibrium and intensify conversion under constrained heat-source temperatures; and (iii) nuclear-assisted reforming, which supplies low-carbon heat and electricity (via SMRs/advanced reactors) and motivates integrated process designs and benchmark comparisons.

i) Electrified SMR

Commercial-scale validation of eSMR technology has been successfully demonstrated in industrial applications Refs. [5–7]. A prime example is Topsoe's eREACT™ pilot plant, Ref. [8], which has

conclusively proven the viability of electrified reforming under real operating conditions. The facility consistently achieves near-equilibrium syngas production across a practical operating window of 750-1000°C and 3–20 bar, with measured electricity-to-process efficiencies of 72–80% at 10 bar. Operational data confirms the system's rapid thermal response, reaching operating temperatures (630 → 900°C) in just 2.6 h, while maintaining continuous stable operation for 1050 h. Perhaps most compelling are the scale-up projections, which indicate over two orders of magnitude reduction in reactor (furnace) volume (e.g., a conventional ~1,100 m^3 side-fired reformer (~2,230 kmol H_2/h) could be replaced by a single ~5 m^3 electrically heated reformer at comparable conditions (auxiliaries excluded)). Independent pilot-plant data on Topsoe's eREACT™ platform corroborate the feasible operating window and fast thermal response, and report 72–80% measured reactor efficiency at pilot scale (with ≥99% predicted at ≥1 MW), Ref. [5]. Advanced control systems using model predictive control (MPC) with delayed gas chromatograph measurements further demonstrate eSMR's advantages, enabling faster hydrogen setpoint tracking and grid-responsive operation while handling the electrical heating setpoint limits and thermal stress constraints – crucial capabilities for flexible, hybrid heat-power operation, Refs. [9–11].

In Refs. [2,12] techno-economic analyses are presented that reinforce the eSMR potential: direct electrification of the radiant duty at fixed throughput can raise reformer thermal efficiency from ~85.6% to ~88.9% while slashing low-purity flue-gas CO_2 by ~92% (4.553 → 0.387 kg CO_2/kg H_2), and levelized costs as low as $2.47–$2.65/kg have been reported in electrified flowsheets leveraging heat recovery and high-temperature heat pumps, subject to local electricity/gas/carbon prices. The capital cost analysis in Ref. [13] demonstrates that eSMR remains competitive with conventional SMR, as the elimination of combustion systems offsets the higher costs of electrical control components. This cost parity indicates that eSMR capital expenditures (CAPEX) remain comparable to conventional systems at moderate scales.

ii) Membrane-assisted reforming

Steam-methane reforming in a Pd-based fluidized-bed membrane reactor operated in bubbling fluidization (no circulating loop, no cyclone) is investigated in Ref. [14]. It demonstrates two weeks of stable operation with 100% H_2 perm-selectivity up to 630°C and CO-free permeate within gas chromatograph detection limits (<10 ppm). The bench unit, externally heated by three electric furnaces (2.2 kW each), was sized to deliver ~1.5 N-lpm of pure H_2. Tests over 500–630°C and 2.0–5.3 bar showed that higher temperature and pressure increased approach-to-equilibrium conversion and hydrogen yield, whereas raising the steam-to-carbon ratio or the weight hourly space velocity (WHSV), the total mass flow of feed per mass of catalyst, h^{-1}, (i.e., shorter residence time) reduced them, reflecting trade-offs among reaction kinetics, permeation driving force, and transport.

In Ref. [15], a cyclone-decoupled, external nickel (Ni) membrane loop is shown to provide a robust and economical separation architecture for high-temperature SMR. The bubbling bed operates conventionally while a primary cyclone removes entrained solids; the hot, dust-lean gas is routed to an external Ni membrane module for hydrogen withdrawal, and the retentate is recycled to the reactor. Dense/supported Ni offers high selectivity to H_2 relative to larger reforming species but lower permeability than Pd-alloys; thus, practical designs typically compensate with larger installed area and, where helpful, a sweep on the permeate side. Under SMR-typical conditions (i.e. bed/retentate pressures on the order of 700–1500 kPa and permeate 100–400 kPa with sweep or mild vacuum) the hydrogen flux follows Sieverts' law. It is limited primarily by effective thickness, yielding order-of-magnitude fluxes that are modest compared with Pd. The principal advantages are low material cost, good high-temperature mechanical stability, and intrinsic reforming activity; trade-offs include a smaller per-module equilibrium shift and greater reliance on recycle to achieve deep CH_4 conversion (pressures and sweep-side operation consistent with Ref. [15]. As a ballpark (very design-dependent), thin supported Ni films might deliver only ~0.005–0.03 mol/m^2·s at 600–700 °C with a moderate pressure split, while dense tubes are lower. Pros: lower cost metal, good high-T stability, intrinsic SMR catalysis, and better tolerance to occasional solids carryover; cons: more membrane area, typically smaller equilibrium shift per module, and more recycle duty to reach deep CH_4 conversion.

For maximum equilibrium shift and compact, high-purity hydrogen production, a Pd-alloy membrane placed outside the fluidized solids, again downstream of a cyclone in a protected side loop, is generally preferred. Thin supported Pd-alloy layers (≈5–10 μm effective thickness) provide near-ideal H_2 selectivity and substantially higher permeability, enabling order-of-magnitude higher mass fluxes than Ni at 550–700°C for similar $\Delta\sqrt{P}$ (e.g., retentate ≈700–1500 kPa, permeate 100–400 kPa with sweep), which translates into stronger conversion enhancement and reduced reactor/catalyst inventory. The trade-offs are higher metal costs and stricter requirements for sulfur/poisoning and thermal management to prevent defect formation and embrittlement; placing the membranes in a cyclone-decoupled external module mitigates abrasion and thermal cycling risks while preserving the separation benefit. Overall, a Pd-alloy membrane in a cyclone-protected side loop is the performance-oriented choice. In contrast, a Ni-based loop prioritizes mechanical resilience and cost with acceptable, though lower, flux and equilibrium shift, Ref. [15].

A pilot fluidized-bed membrane reactor (FBMR) for SMR and water–gas shift (WGS) reactions using 10 Pd H_2-selective tubes is investigated in Ref. [16]. The process is conducted in a 10 cm-ID, 60 cm-tall vessel electrically heated by three 2.2 kW furnaces, operated at 1.5–6 u/umf, 550–650°C, and 2–4 bar. By selectively withdrawing hydrogen, the FBMR surpasses equilibrium limits, raising CH_4 conversion, lowering CO selectivity, and increasing H_2 yield, with ultrapure permeate suitable for PEM fuel cells (<10 ppm CO). At 550°C and 2 bar, the unit delivered about 53–61 W equivalent H_2, with separation factors rising from ~0.57 to ~0.80 as throughput increased. Performance improved with higher temperature and pressure, and a two-phase model matched the data when axial back-mixing was negligible, indicating plug-flow-like behavior with membrane permeation as the governing limitation. The study validates small-scale process intensification and points to future autothermal bi-membrane designs that couple an O_2-permeable partial-oxidation stage beneath the SRM/WGS/membrane section.

Early work by Ref. [17] established the design space for steam-methane reforming in fluidized-bed membrane reactors (FBMRs), combining a two-phase bubbling-bed model with Xu–Froment kinetics and Sieverts-law H_2 permeation to interpret and extend bench data from a Pd-tubed FBMR. They compared co-current and countercurrent configurations and showed that, with high-flux thin Pd films and favorable pressure splits, countercurrent operation is generally superior for longer beds (achieving complete CH_4 conversion in the model), whereas co-current can be advantageous for short beds at lower temperatures; they also quantified how sweep gas and lower permeate-side pressure strengthen the driving force for H_2 removal, how higher reaction-side pressure can improve conversion in FBMRs despite equilibrium penalties in conventional fluidized bed reactors (FBRs), and how membrane thickness strongly impacts performance. This analysis positions FBMRs as a complementary intensification route, shifting equilibrium in situ and producing ultrapure H_2, highly relevant to electrified architectures where heat supply can be decoupled from separation.

A model of a hydrogen-selective fluidized-bed membrane reactor operating in the bubbling regime (two-phase bubble–emulsion with a dilute freeboard), not a circulating loop, is reported in Ref. [18]. The reactor embeds a bundle of high-flux H_2-selective tubular membranes (Pd-type behavior via a Sieverts-law permeation correlation; 18 tubes, ~3.175 mm OD, permeate-side pressure ~0.14 MPa with ~45 mol/h sweep) in the upper bed/freeboard to withdraw H_2 and shift

equilibrium. Under identical baseline conditions (900 K, ~0.99 MPa), adding membranes lifts CH_4 conversion from ~0.59 to ~0.71 and raises H_2 yield from ~2.25 to ~2.71 mol H_2 per mol CH_4. At the modeled lab scale, the feed is ~45 mol/h CH_4 with ~138 mol/h steam, and, for combined SMR and dry reforming of methane (DRM) cases, ~45 mol/h CO_2, giving permeate hydrogen flows on the order of ~14–48 mol/h depending on the operating point. The optimization further shows that coupling SMR with DRM in this FBMR enables tuning syngas to $H_2/CO \approx 1$ at higher CH_4 conversion than pure SMR (albeit with less total H_2), illustrating FBMR's utility for equilibrium shifting, coking mitigation via steam/CO_2 ratios, and product tailoring.

An FBMR for SMR in modeled Aspen Plus by "unfolding" the reactor into repeated sub-reformer/sub-separator pairs, as reported in Ref. [19]. Each sub-reformer is an RGIBBS (equilibrium) block for SMR/WGS, and each sub-separator is a custom FORTRAN unit implementing Sieverts-law H_2 permeation; the model assumes 1-D plug flow with uniform temperature and negligible pressure drop, and takes as key inputs the membrane permeation capacity (area/thickness), mixed-gas effectiveness factor, permeation pre-exponential and activation energy, reactor P-T-S/C, and permeate-side H_2 pressure (often reduced by vacuum). Using >50 separator stages makes results insensitive to stage count. Two representative capacities are reported: 1) a "typical" sensitivity case at 1 kmol/h CH_4 feed at 600°C, 2 MPa, steam-to-carbon ratio of 3, hydrogen permeate pressure of 100 kPa, and 2) a validation case against the a pilot reformer (Ø ≈97 mm × 1.143 m, 12 Pd tubes) for74.2 mol/h CH_4 feed. In those cases, H_2 production increases from ≈1.7 to ≈6.3 mol/h as the bed temperature increases from 457 to 640°C. Overall, the RGIBBS + Sieverts workflow captures how in-situ H_2 withdrawal shifts equilibrium, boosts H_2 yield, and can even reverse the adverse pressure effect at sufficient permeation capacity, providing a practical design tool before introducing detailed hydrodynamics.

An Aspen Plus model of a nickel-based fluidized-bed membrane reactor (FBMR) for SMR is developed in Ref. [20] by splitting the unit into repeated equilibrium sub-reformers (RGIBBS blocks for SMR/WGS) and user-defined sub-separators that compute H_2 flux via a Sieverts-law membrane module implemented through Aspen's User Model interfaced to Excel. The workflow assumes 1-D plug flow, isothermal operation, negligible pressure drop, and local reaction equilibrium, with key inputs including membrane permeation capacity (area/thickness), a mixed-gas effectiveness factor, permeation pre-exponential (k) and activation energy (E), reactor P–T–S/C, and permeate-side H_2 pressure (often reduced by sweep/vacuum). The framework is validated against an experimental Pd-FBMR pilot reformer (Ø≈97 mm × 1.143 m, 12 tubes; CH_4 = 74.2 mol/h, steam = 178.1 mol/h, sweep ≈80 mol/h, P≈980 kPa), reproducing methane conversion (~11–42%) and H_2 production (~1.7 → 6.3 mol/h as 447 → 913°C) and showing that > 50 separator stages render results insensitive to discretization. Parametric studies indicate that, at comparable conditions, Ni membranes ($k \approx 1.44 \times 10^{-6}$ mol/m·s·Pa$^{0.5}$, $E \approx -51$ kJ/mol) require much larger area to match Pd performance due to lower permeability: achieving ~68% CH_4 conversion with ~1.86 mol H_2/mol CH_4 needs ~49 m^2 Ni versus ~8 m^2 Pd (~6.1 × more), though Ni's higher temperature stability and far lower material cost can offset this at scale. Pressure, temperature, and permeate-side H_2 pressure trends follow expectations for FBMRs—membrane removal of H_2 counters equilibrium penalties and can even reverse the adverse pressure effect at sufficient permeation capacity—providing a practical Aspen-based tool for sizing membrane area and exploring operating windows before detailed hydrodynamics.

A circulating fast fluidized-bed membrane reformer (CFFBMR) is proposed in Ref. [21] coupling steam reforming with oxidative reforming while integrating palladium H_2-selective membranes for in-situ hydrogen removal and perovskite oxygen membranes for distributed O_2 feed, enabling autothermal operation and equilibrium shifting. Using a 1-D plug-flow model with Xu–Froment SMR kinetics and literature oxidative reforming kinetics, isothermal and adiabatic simulations (baseline: CH_4 ≈3.95 kmol/h, S/C ≈3.56, catalyst dp ≈186 μm, Pd layer ≈20 μm, tube L ≈2 m, ID ≈0.0978 m) show that adding H_2 membranes raises CH_4 conversion at 900 K and ~0.5 MPa from ~0.56 to ~0.964 and lifts H_2 yield from ~2.05 to ~3.71 mol/mol; at higher pressure (~1520 kPa) the membrane reactor reverses the usual adverse pressure effect, reaching total H_2 yields ≈3.93. Introducing oxygen, either directly or via O_2 membranes, provides endothermic heat, smooths temperature profiles, and enables near-isothermal, autothermal operation with an optimal O_2/CH_4 ratio of ~0.28–0.33; optimization at 727°C and 500 kPa yields a total H_2 yield ≈3.20. Versus an industrial fixed-bed SMR (13.72 m tubes), the optimized CFFBMR (2 m) improves yield (3.373 vs 2.812 mol/mol), slashes reactor volume (0.015 vs 0.103 m^3), eliminates the fired furnace, and boosts hydrogen productivity to ~8.2× (≈8.89×10^5 vs 1.08×10^5 mol H_2/h·m^3), highlighting strong process-intensification potential.

In Ref. [22], a steady-state FBMR model that couples a two-phase bubbling-bed description (bubble + dense phases with limited dense-phase plug flow) to palladium-type H_2 permeation (Sieverts law) through immersed tubes is presented. The system includes plug flow of sweep/permeate inside the tubes, and accounts for freeboard reactions over entrained catalyst; reactions follow Xu–Froment SMR/WGS kinetics and the coupled bed–membrane–freeboard ordinary differential equations (ODEs) are solved numerically and validated against pilot data from a 102 mm-ID unit rated at ~6 m^3(STP) H_2 per h (447–657°C, ~690–980 kPa), giving mean absolute conversion errors ~2.4% with permeation and ~4.2% without. Parametric studies span 400–800°C, 0.3–2.7 MPa, S/C = 1.5–5.5, CH_4 = 20–100 mol/h, membrane equivalent permeation capacity C_{ep} = 0.4–7.0 km (kilometers of equivalent permeation length), sweep = 40–120 mol/h, and permeate-side pressure = 100–900 kPa, showing:

a. temperature and C_{ep} strongly raise conversion, with ~0.96 at 800°C and 2700 kPa when C_{ep} is high (exceeding equilibrium by ~25%);
b. pressure can increase conversion in FBMRs (opposite fixed-beds) because higher total pressure boosts permeation driving force;
c. increasing S/C raises conversion but lowers the fraction of H_2 removed (weaker equilibrium shift);
d. higher throughput reduces conversion as membrane removal becomes rate-limiting;
e. more sweep modestly helps, while increasing permeate-side pressure modestly hurts (≈4% conversion drop across a ninefold increase); and
f. placing some membrane area in the freeboard suppresses reverse reactions there.

The sensitivity tests indicate that the conversion is only weakly affected by bubble solids content, gas split between phases, catalyst activity, or bubble size under the studied conditions, highlighting that thermodynamics plus selective H_2 withdrawal dominate FBMR performance.

iii) Nuclear-assisted reforming

Nuclear-assisted reforming is relevant not only as a decarbonization option, but also as a concrete industrial application of advanced reactors, because refinery and petrochemical sites require the same combination of continuous steam, process heat, and electricity that SMNR cogeneration systems are designed to supply. Nuclear-assisted SMR extends this trajectory by supplying low-carbon heat and electricity from reactors ranging from today's light-water reactors (LWRs) to Gen-IV concepts like high-temperature gas-cooled reactor (HTGR) and molten-salt reactor (MSR), Refs. [23–26]. Small Modular Nuclear Reactors (SMNRs), including light-water (LWR), liquid–metal-cooled (LMR), molten-salt (MSR), and gas-cooled (GCR/HTGR) designs, are inherently well suited to supply refinery and petrochemical sites with reliable, low-carbon steam and power Ref. [26]. Their compact, modular plants couple with standard balance-of-plant equipment (steam generators, reheaters, turbines) and can be tailored for cogeneration, with one steam header serving a turbine train and another serving process users

(strippers, reboilers, hydrogen units). All those reactors can be engineered to deliver high-pressure steam across the 50–200 atm range and, where reactor outlet temperatures permit, superheated steam with ≥350°C of superheat for power cycles and high-grade process heat. Integration is flexible: a single SMNR can run mixed-pressure headers, e.g., high-pressure (HP) to the turbine and medium/low-pressure (MP/LP) to process, support rapid load-following via steam-bypass trains, and backstop grid volatility while decarbonizing onsite boilers.

Steam conditions are determined by the reactor outlet temperature and the heat exchanger design. Light water reactor SMNRs typically produce saturated HP steam around 50–80 atm and ~280–300°C; adding nuclear-powered or hybrid superheaters in the secondary can raise temperatures to ≥350°C for turbine admission while maintaining nuclear-grade pressure boundaries. LMR (sodium or lead) and HTGR units routinely support superheated steam at ~100–150 atm and 480–600°C, well matched to modern reheat turbines and energy-intensive process duties. MSRs with 600–700°C primary salt likewise enable ≥350°C superheat at HP conditions and can be configured for even higher temperatures, subject to material limits. In short, across LWR, LMR, MSR, and GCR families, SMNRs are adaptable to furnish superheated steam at 50–200 atm (or higher where warranted) with superheat from ~350°C upward, providing a drop-in, low-carbon replacement for fossil-fired boilers and a robust heat source for both power generation and refinery processes.

Small modular nuclear reactors (SMNRs), particularly high-temperature gas-cooled designs (HTGRs), offer steady, low-carbon heat and electricity that can directly energize steam-methane reforming (SMR). Building on this idea, a helium-heated membrane reformer tailored for HTGR coupling is modeled in [27], noting that the secondary helium typically available (≈700–900°C at ~4000 kPa) is cooler than top-fired petrochemical furnaces. To compensate, the system embeds a hydrogen-permeable sweep tube inside a triple-tube catalytic geometry so in-situ H_2 removal drives SMR/WGS forward, lifting conversion and H_2 yield at lower heat-source temperatures. Using a 1-D reaction–flow model validated against prior data, Ref. [27] shows that the membrane reactor (MR) consistently outperforms an equivalent reformer tube (RT): for the same hydrogen production, a 6 m MR matches a 9 m RT, and a 9 m MR exceeds a 27 m RT, underscoring major compactness and efficiency gains. The study also quantifies how sweep ratio, sweep-side pressure, and membrane thickness govern performance, recommending thin, high-flux membranes and adequate H_2 partial-pressure difference to maximize yield while maintaining operability, together making HTGR-coupled MRs a promising pathway for nuclear-assisted, low-carbon hydrogen.

Nuclear-heated SMR by coupling medium-temperature reactor heat (~550°C) to a recirculating Pd-membrane reformer that performs reforming, shift, and H_2 separation in one unit is reported in Ref. [28]. The originality lies in the use of a closed-loop membrane architecture for nuclear integration to strengthen the H_2 driving force, shrink membrane area and plant size, and simplify CO_2 capture. The study contrasts conventional fired tubes at 700–800°C with the integrated membrane reformer operating effectively at ~500–550°C. Cited demonstrations, Ref. [28], include Tokyo Gas/MHI units (e.g., ~15 Nm^3 H_2 per h for ~1,500 h; typical ~21.8 Nm^3 H_2 per h at 550°C, ~830 kPa, 99.999% purity), underscoring membrane feasibility. System metrics highlight "synergy": H_2 heat output ≈330% of the reactor heat input and ≈115% of methane LHV input, with an overall H_2-to-(nuclear + CH_4) heat ratio near 85%, implying ~30% reductions in methane use and CO_2 versus fired SMR while remaining closer to commercialization than high-temperature thermochemical cycles.

A first-principles, dynamic two-dimensional model of a nuclear-heated steam methane reforming (SMR) tube bundle is developed in Ref. [29]. The model resolves shell-side helium, refractory insulation, tube walls, tube-side reacting gas, and intra-particle diffusion and heat transport explicitly (no effectiveness factors), and it includes an inner heat-recovery tube. The governing partial differential–algebraic equations (PDAEs) are discretized using finite differences and solved in gPROMS (General PROcess Modeling System), an equation-oriented dynamic simulator, achieving strict component mass conservation and an overall energy-balance error of about 0.25 percent with a suitably refined grid. Validation is performed against designs from the Japan Atomic Energy Research Institute (JAERI), including the High-Temperature engineering Test Reactor (HTTR) program: the model matches design targets of about 120 Nm^3 H_2/h (single-tube mock-up) and about 4200 Nm^3 H_2/h (30-tube HTTR bundle).

The model is then applied to an industrial High-Temperature Reactor (HTR)-Module concept (helium coolant 950°C, 50 atm; process-gas feed 34.8 kg/s; 199 tubes, 0.12 m ID, 14 m length; steam-to-carbon ratio S/C = 4), predicting helium cooling duty about 72.9 MW, syngas outlet about 853°C, inner-tube exit about 591°C, and about 73% CH_4 conversion with 6.3 H_2/CO ratio. Because radiative heat transfer is relatively weak at nuclear primary-helium wall temperatures, disc-finned inner tubes are employed to boost convection. Disturbance studies show weak sensitivity to a +100 K process-gas inlet step (approximately +1.2 percentage points conversion, with lower duty) but strong sensitivity to a +100 K helium inlet step (approximately +15 percentage points conversion, +18.5 percent duty). Parameter sensitivities (±20% in particle size and tube/shell dimensions) modestly affect conversion (±4.9%) and duty (±2.7%) while barely changing outlet temperatures (<0.7%), supporting the robustness of nuclear-integrated SMR designs and providing a sound platform for control and scale-up.

The economics of supplying SMR process heat with either high-temperature gas-cooled reactors (HTGRs) or solar towers is evaluated in Ref. [30] versus a conventional fossil heater, using a mixed-integer linear optimization with hourly resolution to size and dispatch HTGR modules (250 MW_{th}, 850°C), solar towers with ceramic sensible-heat storage and electric reheaters, a steam turbine, and electricity purchases/sales, for a constant 12.73 tH_2/h plant in Huelva, Spain (2015 prices; SMR includes CO_2 capture, while the fossil heater vents CO_2). Base-case hydrogen costs are: fossil $2.19/kg; nuclear (two HTGRs + turbine) $3.53/kg; nuclear + fossil backup $2.81/kg; pure solar $5.54/kg (ten ~200 MW_{th} towers + ~41 GWh_{th} storage, dominated by reheating losses); solar + fossil $3.40/kg (seven towers, ~6.1 GWh_{th} storage); and solar + nuclear $4.10/kg. Sensitivity runs show that with gas at $67.00/MWh and CO_2 at $29.18/t, nuclear + fossil becomes cost-competitive with fossil ($3.63 vs $3.71/kg), and with gas at $100.50/MWh and CO_2 at $58.37/t, pure nuclear ($5.09/kg) and solar + fossil ($5.23/kg) also edge out fossil ($5.29/kg).

Song et al., Ref. [31], analyzes a baseline power-to-power pathway using electrolysis and compares it with an alternative that stores renewable electricity via electrified steam-methane reforming (eSMR), assessing whether the latter attains superior efficiency and cost. Two flowsheets are modeled:

(1) EL-GT, which produces and stores H_2 using an ≈60%-efficient electrolyzer and then combusts it in a gas–steam combined cycle (GSCC); and
(2) eSMR-GT, which replaces the electrolyzer with an electrically heated reformer augmented by a high-temperature heat pump and a steam compressor, delivering an H_2-rich syngas to the same GSCC.

Both schemes include monoethanolamine (MEA) CO_2 capture and liquefied natural gas (LNG) cold-energy integration, and performance is swept over the H_2 fraction at the turbine inlet. In storage mode, eSMR exhibits a much lower specific electricity consumption for producing H_2 equivalent (~11.3 kWh per kg H_2 equivalent) than electrolysis (~55 kWh/kg, Ref. [33]), yielding a higher peak round-trip efficiency for eSMR-GT (45.84% vs 30.6%). In generation mode, both pathways benefit from increased H_2 fraction at the turbine inlet, although the ESMR-GT syngas slightly increases steam demand in the MEA unit. Overall, eSMR-GT requires substantially less power for CO_2 capture

(~11 kWh/tCO_2, 27% of the EL-GT case) and achieves the lowest cost of electricity with CCS ($0.289/kWh, ~11.9% below the electrolyzer-based option). The authors conclude that eSMR-GT is the more efficient and cost-effective route for dispatchable low-carbon power.

iv) Research gap

Despite substantial progress across electrified SMR, membrane-assisted reforming, and nuclear-assisted integration, prior studies typically address these elements in isolation. In particular, the literature rarely combines, on a single consistent plant-gate basis, (i) a reactor-neutral nuclear steam/power supply block, (ii) electrically supplied reforming duty, (iii) cyclone-decoupled external H_2-selective separation integrated with recycle, and (iv) concentrated CO_2 handling with explicit accounting of auxiliary electrical loads and benchmark positioning relative to electrolysis (and, by established literature, to blue-hydrogen comparators). The present work addresses this integration gap by evaluating the combined configuration and reporting the resulting plant-gate energy and CO_2 metrics on a consistent basis.

The studies summarized above are not only relevant for context but also provide the quantitative basis for the NET-SMR model developed in this work. Operating windows, efficiency ranges, membrane permeation capacities, and reactor compactness factors are taken from Refs. [5–7,15–17,19–22,28–31] to define realistic temperature, pressure, conversion, and efficiency targets and to calibrate the Aspen Plus and EES simulations. In this sense, roughly half of the parametric ranges used in the present model are directly grounded in prior experimental or detailed modeling studies. At the same time, the remaining degrees of freedom are explored to assess the specific nuclear electro-thermal integration proposed here.

3. NET-SMR concept

We consider a generic small modular nuclear reactor (SMNR) and begin by laying out a universal, reactor-neutral steam Rankine power cycle in which the steam generator is partitioned into economizer, evaporator, superheater, and reheater. The cycle is configured to (i) admit demineralized make-up water at the feedwater-heater train to close the Rankine mass balance, (ii) use its feedwater-preheating, boiling, and superheating trains to produce the process steam required by the steam methane reforming (SMR) unit, and (iii) recover sensible and latent heat from SMR product-side coolers to energize the feedwater-preheating train. The primary working fluid loop of the SMNR supplies as much of the economizer/evaporator/superheater/reheater duty, including make-up-water preheating, as allowed by its outlet temperature and pinch constraints. Electric heaters provide any remaining superheat/reheat. If a LWR is to be used as SMNR, the electric heaters cover essentially all superheat (and often part of evaporation at very high pressures); for high-temperature SMNRs such as sodium-fast reactor (SFR), lead fast reactor (LFR), MSR, HTGR, the coolant can supply full preheat/boil and most or all superheat, with electric heaters reserved for trim or fast load-following.

The target primary steam conditions used here are $P_{HP} = 150$ atm (where HP stands for high pressure steam) with a superheat margin $\Delta T_{sup} = 200^{\circ}$C, representative of current SMNR concepts, summarized in the Litetrature Review section. These steam-pressure and superheat targets, together with the reactor-neutral cogeneration configuration adopted here, are consistent with recent advanced-nuclear integration studies and with the reported steam-delivery capabilities of current SMNR concepts Refs. [23,24,26,30]. The SMNR balance-of-plant arrangement is shown schematically in Fig. 1.

Process steam is withdrawn as a controlled extraction from the high-pressure turbine, combined with preheated natural gas at the target steam-to-carbon ratio, and then brought to SMR inlet conditions in two stages: (i) nuclear-derived process heating and (ii) final electrical energization by Joule heating to the reforming temperature.

4. Model formulation

Mass and energy balance equations for all devices are used to model

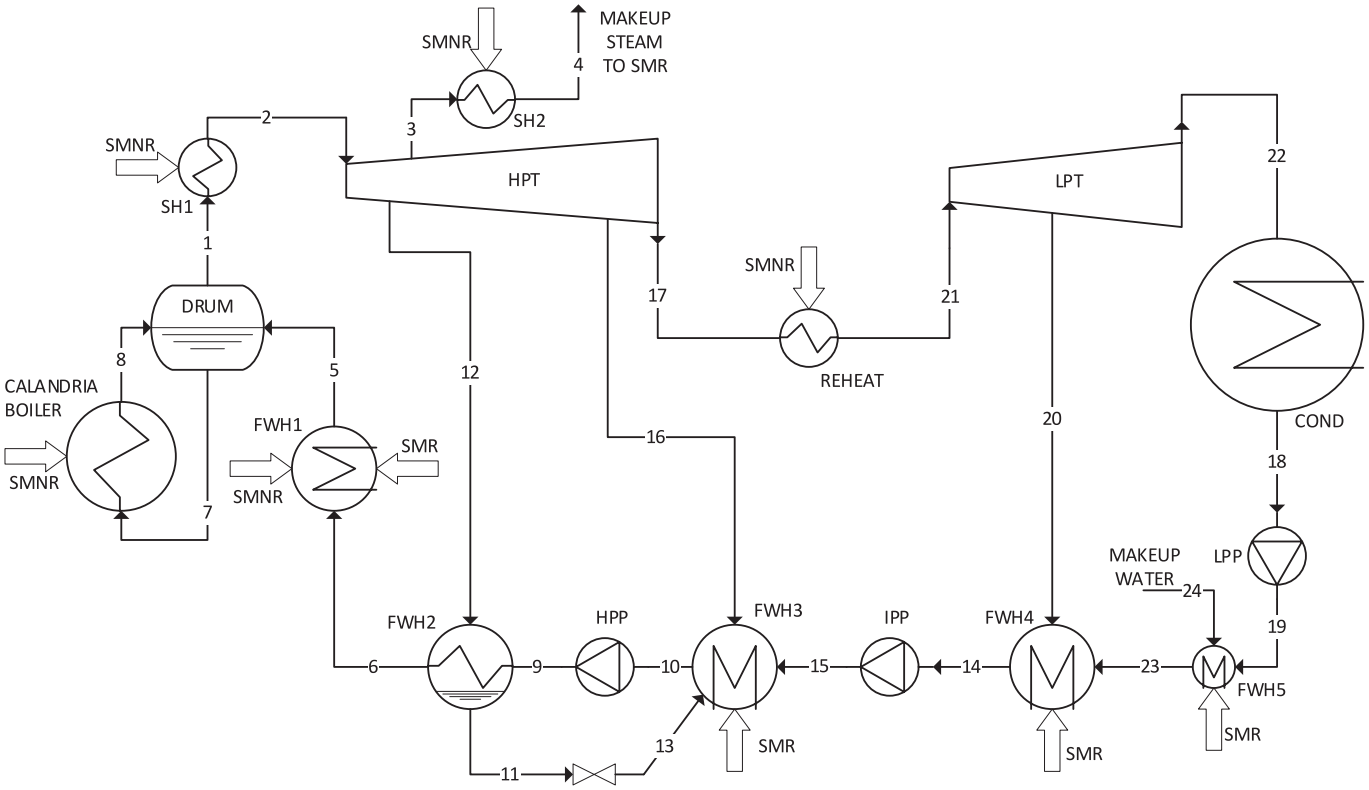

Fig. 1. Balance of plant of the SMNR to provide process steam and electric power.

the power cycle, which is coded in Engineering Equation Solver [32]. The enthalpy of steam 1 corresponds to saturated high-pressure steam above the drum. The high-pressure steam $P_1 = P_{HP}$ fixes the saturation temperature T_1. The superheating degree ΔT_{sup} fixes temperature $T_2 = T_1 + \Delta T_{sup}$. The temperatures, pressures, and vapor quality provide the enthalpies and entropies of steam at streams 1 and 2. The energy balance equation determines duty of SH1:

$$\dot{m}_1 h_1 = \dot{m}_2 h_2 + \dot{Q}_{SH1} \tag{1}$$

The mass and energy balances on the high-pressure turbine require, HPT:

$$\begin{cases} \dot{m}_2 = \dot{m}_{12} + \dot{m}_3 + \dot{m}_{16} + \dot{m}_{17} \\ \dot{m}_2 h_2 = \dot{m}_{12} h_{12} + \dot{m}_3 h_3 + \dot{m}_{16} h_{16} + \dot{m}_{17} h_{17} \end{cases} \tag{2}$$

After generating work steam, stream 3 is extracted at a convenient pressure for steam methane reforming (32 atm) and heated up to $T_4 = T_2$, following the usual cogeneration practice of extracting process steam from an intermediate turbine stage. On the figure SMNR indicates heat inputs derived from the nuclear reactor. The mass and energy balance on the low-pressure turbine, LPT, reads:

$$\begin{cases} \dot{m}_{21} = \dot{m}_{20} + \dot{m}_{22} \\ \dot{m}_{21} h_{21} = \dot{m}_{20} h_{20} + \dot{m}_{22} h_{22} \end{cases} \tag{3}$$

The turbines are modeled via a constant isentropic efficiency, taken as $\eta_S = 0.9$ as a representative design assumption for the present conceptual study:

$$\eta_S = \frac{h_{in} - h_{out}}{h_{in} - h_{s=ct.}} \tag{4}$$

The thermal energy of the nuclear reactor is transferred primarily to the calandria boiler:

$$\dot{Q}_B = \dot{m}_7 (x_8 - x_7) \Delta h_{LV} \tag{5}$$

in which the boiler-exit vapor quality is taken as $x_8 = 0.1$ as a representative calandria-boiler recirculation design assumption, while $x_7 = 0$ and Δh_{LV} is the latent heat of water vaporization.

The preheater FWH1 is designed to be energized mainly from the nuclear reactor, and additionally from heat recovery provided from the integrated SMR process which is introduced latter. The total duty of FWH1 is given by:

$$\dot{Q}_{FWH1} = \dot{m}_6 (h_5 - h_6) \tag{6}$$

The energy balance on the feed water heater FWH2 determines the flow rate of extracted high-pressure steam $\dot{m}_{12}$ under the design-imposed constraint that the steam is fully condenses, i.e., $x_{11} = 0$:

$$\dot{m}_9 h_9 + \dot{m}_{12} h_{12} = \dot{m}_6 h_6 + \dot{m}_{11} h_{11} \tag{7}$$

The pressure in extracted steam, stream 12, is to be determined by a parametric study as a compromise between targeting high power generation magnitude and targeting high power generation efficiency, which are contradictory objectives. The feed water heaters FWH3, FWH4, FWH5 are all energized by heat transfer from the SMR process. At FWH5 makeup water is introduced as stream 24. The feed water heaters FWH3, FWH4, FWH5 are all energized by heat transfer from the SMR process. At FWH5 makeup water is introduced as stream 24. Makeup demineralized water is admitted at the low-pressure feedwater heater FWH5 (streams 23–24), analogous to a condenser hotwell/deaerator, while saturated steam for the SMR makeup is extracted from the high-pressure turbine at the appropriate stage (streams 3–4), in line with standard power–process cogeneration practice in refineries. The energy balance on the feed water heaters is:

$$\begin{cases} \dot{m}_{15} h_{15} + \dot{m}_{16} h_{16} + \dot{m}_{13} h_{13} + \dot{Q}_{SMR.3} = \dot{m}_{10} h_{10} \\ \dot{m}_{23} h_{23} + \dot{m}_{20} h_{20} + \dot{Q}_{SMR.4} = \dot{m}_{14} h_{14} \\ \dot{m}_{19} h_{19} + \dot{m}_{24} h_{24} + \dot{Q}_{SMR.5} = \dot{m}_{23} h_{23} \end{cases} \tag{8}$$

Saturated water is assumed at pumps suction, steams 18, 14, 10. Therefore, the corresponding specific volume v_{18}, v_{14}, v_{10} is calculated based on water pressure and zero vapor quality. The efficiency of all pumps is taken as $\eta_P = 0.9$ as a representative design assumption, and all pumps are modeled on that fixed-efficiency basis as follows:

$$\eta_P = \frac{h_{disch} - h_{suc}}{v_{suc}(P_{disch} - P_{suc})} \tag{9}$$

where subscript "suc" identifies pump suction, while "disch" is the discharge.

The net heat input to the power cycle is given by the sum of all heat inputs:

$$\dot{Q}_{in} = \dot{Q}_B + \dot{Q}_{SH1} + \dot{Q}_{FWH1} + \dot{Q}_{FWH3} + \dot{Q}_{FWH4} + \dot{Q}_{FWH5} + \dot{Q}_{REHEAT} \tag{10}$$

The work of the turbines and the net generated work is calculated by:

$$\begin{cases} \dot{W}_{LPT} = \dot{m}_{20}(h_{21} - h_{20}) + \dot{m}_{22}(h_{21} - h_{22}) \\ \dot{W}_{HPT} = \dot{m}_2(h_2 - h_{12}) + \dot{m}_2(h_2 - h_3) + \dot{m}_2(h_2 - h_{16}) + \dot{m}_2(h_2 - h_{17}) \\ \dot{W}_{NET} = \dot{W}_{LPT} + \dot{W}_{HPT} \end{cases} \tag{11}$$

The power generation efficiency is determined by:

$$\eta_{PG} = \frac{\dot{W}_{NET}}{\dot{Q}_{in}} \tag{12}$$

There are two contradictory objectives for the SMNR balance of plant, namely to maximize $\dot{W}_{NET}$ and to maximize η_{PG}. The reaching of these can be studied under constraints, one of which is fixing the boiler duty, $\dot{Q}_B = fixed$. Other constraint is that the minimum pinch point on the heat exchanger is fixed $\Delta T_{pinch} = 15^{\circ}C$, and the steam extractions at streams 12, 16, 20 impose the mass flow rate be superior to zero. The heat recovered from the SMR flowsheet is determine according to the required heat rejection and imposed as a fixed constraint for the Rankine cycle design, and then taken fixed as well in the optimization studies, $\dot{Q}_{SMR} = fixed$. This will give Pareto frontiers for two-objectives optimization under constraints as expressed follows:

$$F_{obj} = \max\{\eta_{PG}, \dot{W}_{NET} | \dot{Q}_B = fixed, \dot{Q}_{SMR} = fixed, \Delta T_{pinch} \geq 15^{\circ}C, \dot{m}_{12,16,20} > 0, T_6, T_{10}, T_{14}, T_{17}\} \tag{13}$$

Entropy balance equations were used to determine the entropy generation of devices and units of operation and so, to quantify the irreversibility and to validate process feasibility according to the second law of thermodynamics (i.e., entropy generation must be positive for all irreversible processes). Here, is the general form of the entropy balance:

$$\underbrace{\sum \dot{m}_{in} s_{in} + \sum \frac{\dot{Q}_{in}}{T_{in}}}_{\dot{S}_{in}} + \dot{S}_{gen} = \underbrace{\sum \dot{m}_{out} s_{out} + \sum \frac{\dot{Q}_{out}}{T_{out}}}_{\dot{S}_{out}} \tag{14}$$

For individual units of operation and the overall flowsheet, exergy destruction rate is determined by the difference of entropy output and entropy input multiplied by a reference temperature, T_0:

$$\dot{E}x_d = T_0 \dot{S}_{gen} \tag{15}$$

The exergy input is determined from the sum:

$$\dot{E}x_{in} = \sum \dot{m}_{in} ex_{in} + \sum \left(1 - \frac{T_0}{T_{in}}\right) \dot{Q}_{in}, \text{ with } ex_{in} = h - h_0 + T_0(s - s_0) + ex^{ch} \quad (16)$$

Here subscript 0 indicates reference environment, and superscript "ch" indicates the chemical exergy. The exergy efficiency is determined based on exergy input and exergy destroyed:

$$\eta_{ex} = 1 - \dot{E}x_d / \dot{E}x_{in} \quad (17)$$

5. Key assumptions and system boundary

Superheated steam, stream 4 is mixed with preheated natural gas to form the makeup gas to the steam methane reforming process. A preheating train of the makeup gas is developed in ASPEN Plus, as shown in Fig. 2. Nuclear derived heat is used to preheat natural gas in a relatively small heat exchanger under the design condition that $T_{26} = T_4$; after which the gas and steam are mixed and further heated using heat recovery from the SMR loop. The heat recovery heat exchanger HR-HEAT is energized by a hot effluent of SMR process, as will be shown latter. Therefore, the temperature of the gas reactant is lifted to T_{26}, i.e., the required temperature level for steam methane reaction. The natural gas flowrate is calculated in ASPEN plus in accordance to the flow rate of makeup water and the target production capacity of hydrogen. The calculation depends on the specific composition of natural gas, that can vary, depending on the purification process. The SMR makeup natural gas is high in CH_4 content and as low as possible in sulfur, even with no sulfur to avoid catalyst poisoning.

Refined natural gas (pipeline gas) must be purified carefully to obtain the SMR-purified natural gas. Table 1 documents the composition of unrefined, refined and purified natural gas, for the purpose of modeling within this paper. Once the composition of the natural gas is assumed, the molar flow rate of reacting species, mainly CH_4, but also other hydrocarbons in minor amount, will determine the makeup water requirement to achieve the desired production. With mass flow rate $\dot{m}_{25}$ so determined, the duty of preheating heat exchangers is calculated. The duty of HR-HEAT heat exchanger is calculated with $\dot{m}_{27}(h_{28} - h_{27})$ and the design set to match with the heat recovery potential from SMR reaction train. For the preheating train flowsheet, the required pump power, heat input and turbine work related to steam generation are determined. Those parameters are required for the overall energy balance on the SMR loop.

Fig. 3 shows the ASPEN Plus flowsheet for modeling the chemical reaction process of electrified steam methane reforming within the NET-SMR integration. While the main reactor receives heat input by electrical means, the water gas shift reactors and heat exchangers reject heat which is recovered to the feed water preheating train of the steam Rankine cycle, as indicated. The SMR outputs a non-pure hydrogen (stream 34) that is further purified according to the ASPEN PlUS

Table 1
Composition ranges for unrefined, refined, purified natural gas.

Species Name	Chemical Formula	Unrefined NG	Refined NG (Pipeline Quality)	SMR-Purified Makeup Gas
Methane	CH_4	50–85%	90–98%	>95% (often ~97–99%)
Ethane	C_2H_6	5–15%	1–6%	<1–2% (Minimized)
Propane	C_3H_8	2–10%	<1–2%	<0.1% (Minimized)
Butanes	C_4H_{10}	1–5%	Trace – <1%	<50 ppm (Minimized)
Pentanes+	C_5H_{12}+	<1–3%	Trace	<10 ppm (Effectively Removed)
Carbon Dioxide	CO_2	1–15%	≤ 2–3%	<2–3% (Tolerated but minimized)
Nitrogen	N_2	1–10%	≤ 1–3%	<1–3% (Tolerated but minimized)
Hydrogen Sulfide	H_2S	<1% to 15%+	≤ 4–16 ppm (odorless threshold)	< 0.1 ppm (100 ppb) (Critically Removed)
Mercaptans, etc.	e.g., C_2H_6S	Trace – Present	~5–10 ppm (Added as odorant)	< 0.1 ppm (100 ppb) (Critically Removed)
Water Vapor	H_2O	Varies (Saturated)	≤ 7 lb/MMscf (Dehydrated)	Dry (Liquid water removed)
Oxygen	O_2	Typically not present	≤ 0.2–1%	<1 ppm (Removed)
Chlorides / Fluorides	e.g., Cl^-	Not typically controlled	Not typically controlled	< 10 ppb (Critically Removed)

Note: Table 1 summarizes representative composition ranges for unrefined gas, pipeline-quality natural gas, and SMR-purified makeup gas, compiled as a modeling basis for the present study rather than as a plant-specific feed specification.

flowsheet presented in Fig. 4. Within ASPEN Plus, the SMR unit is constructed as a hierarchy which includes a fluidized bed reactor with catalysts recirculation and an integrated hydrogen separation membrane, a circulator and a cyclone, as shown in ASPEN PLUS flowsheet shown in Fig. 5.

The reactions implemented for the steam-methane reforming process are given in Table 2. For Aspen Plus, we represent the catalyst particle-size distribution (PSD) as an equal-weight average using a normal distribution with D50 = 200 μm and a standard deviation of 50 μm, which is similar to the class used in the experiments published in Ref. [7]. The ASPEN Plus hierarchy model used in this study (Fig. 5) is built around a fluidized-bed reformer (FBR) that is energized by an explicit electrical

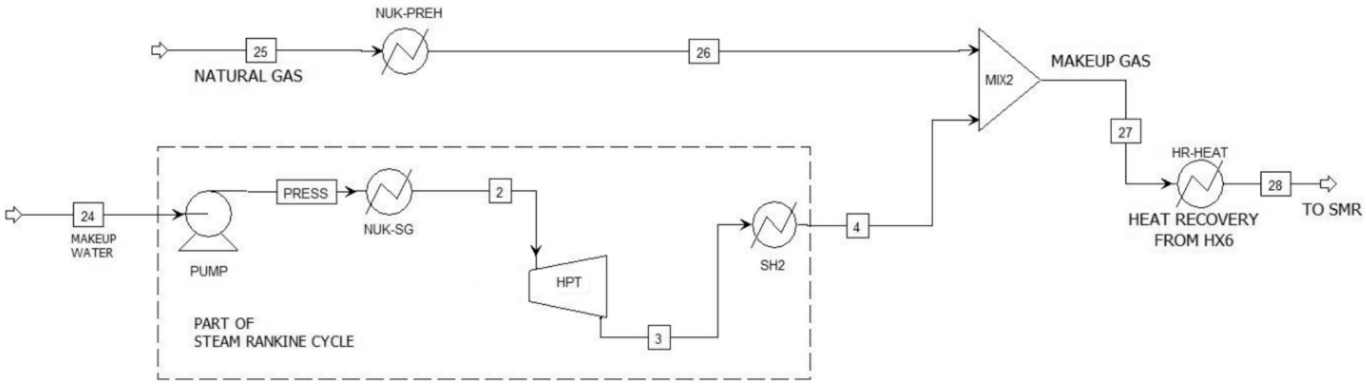

Fig. 2. Preheating train to steam methane reforming process.

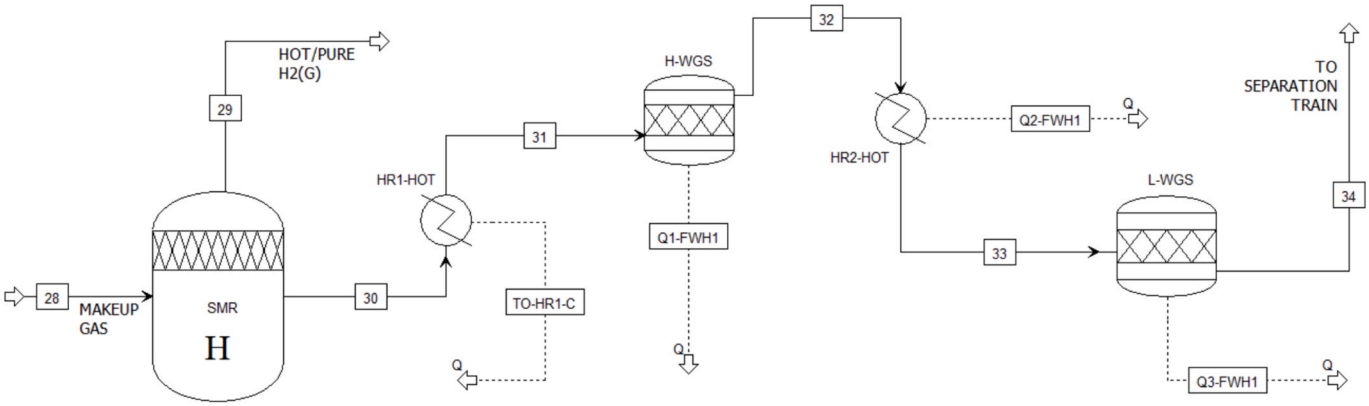

Fig. 3. ASPEN flowsheet for modeling the chemical reaction train within NET-SMR.

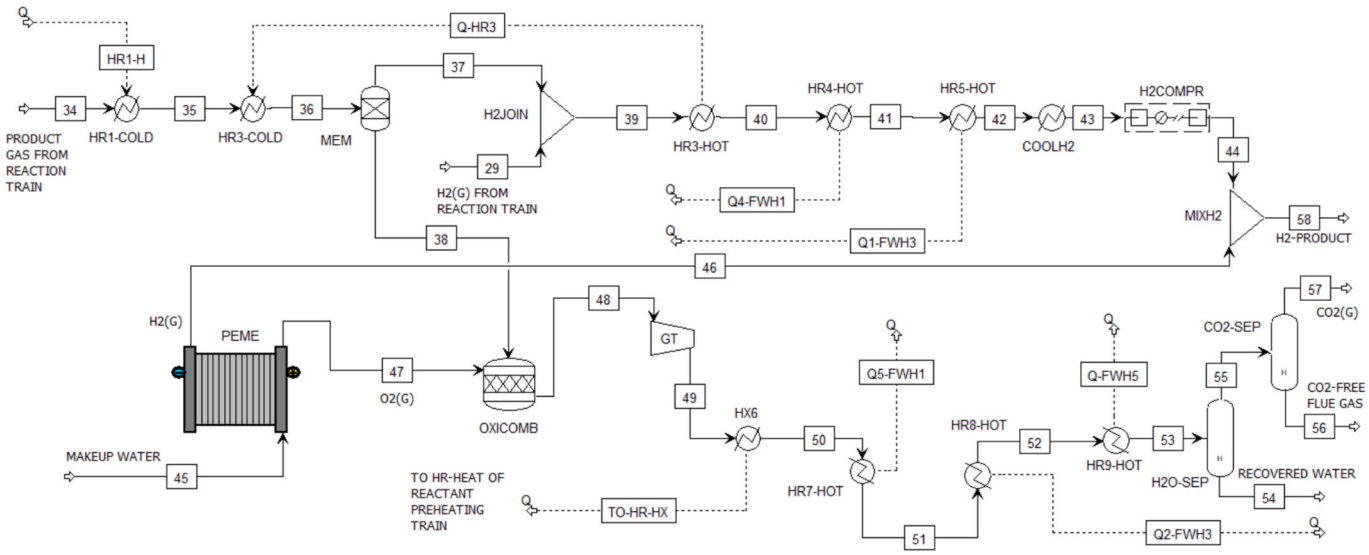

Fig. 4. The separation train to extract pure hydrogen and carbon dioxide from SMR process.

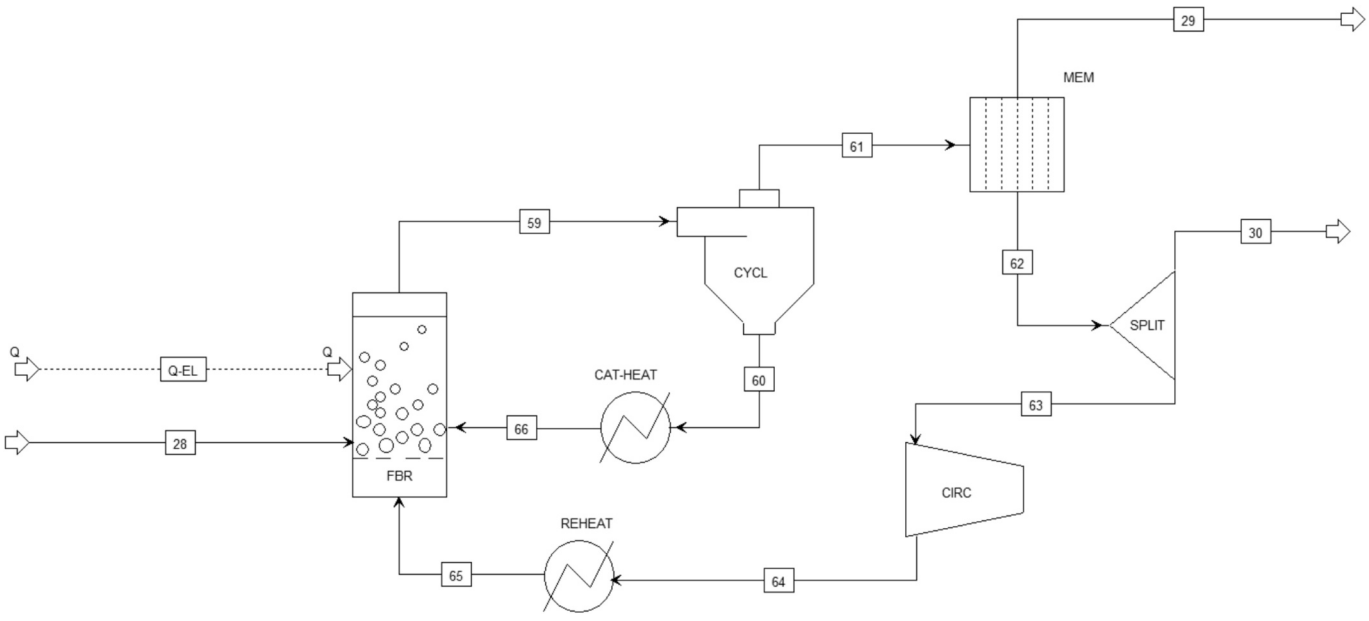

Fig. 5. The SMR hierarchy model of the recirculating fluidized bed reactor for electric-assisted reforming.

Table 2
Most likely reactions in steam methane reforming, [7].

No.	Reaction equation	ΔH° (kJ/mol)	Type of reaction
(1)	$CH_4 + H_2O \rightleftharpoons CO + 3H_2$	+206	Endothermic, equilibrium
(2)	$CO + H_2O \rightleftharpoons CO_2 + H_2$	–41	Exothermic, equilibrium
(3)	$CH_4 \rightleftharpoons C + 2H_2$	+75	Endothermic, forward
(4)	$CO_2 + 4H_2 \rightleftharpoons CH_4 + 2H_2O$	–165	Exothermic, reverse
(5)	$2CO \rightleftharpoons C + CO_2$	–172	Exothermic, reverse
(6)	$CH_4 + 2H_2O \rightleftharpoons CO_2 + 4H_2$	+165	Endothermic, forward
(7)	$C + H_2O \rightleftharpoons CO + H_2$	+131	Endothermic, forward
(8)	$C + 2H_2 \rightleftharpoons CH_4$	–75	Exothermic, reverse
(9)	$CO_2 + C \rightleftharpoons 2CO$	+172	Endothermic, forward
(10)	$CH_4 + CO_2 \rightleftharpoons 2CO + 2H_2$	+247	Endothermic, forward
(11)	$C + O_2 \rightleftharpoons CO_2$	–394	Exothermic, forward

heat input (Q-EL). The fresh makeup reactant feed (stream 28) enters the FBR, where SMR/WGS chemistry is represented and heat is supplied via the Q-EL heat stream. The FBR outlet (stream 59) is routed to a cyclone (CYCL) that performs the gas/solids disengagement required by the circulating solids architecture. In the cyclone, entrained catalyst/solids are removed as a dedicated solids stream (60) and sent to an electrically heated downcomer/solids heater (CAT-HEAT), which restores the solids sensible heat before returning the hot solids to the reactor as stream 66; this closes the catalyst/solids circulation loop and provides a controlled mechanism for distributing electrical heat through the solids phase (in addition to the reactor body heating). The cyclone overhead gas stream (61)—now lean in solids—is sent to the H_2-selective membrane module (MEM), represented in Aspen as a hydrogen-withdrawal separation step that produces a low-pressure permeate hydrogen stream (29) and a high-pressure retentate stream (62). The retentate then enters a splitter (SPLIT) where the net product gas is withdrawn as stream 30, while the remaining fraction is returned as stream 63 to form the gas-phase circulation loop. This recycle stream is driven by a circulator/compressor (CIRC) to restore loop pressure and flow (stream 64), then reheated in an electric reheater (REHEAT) before re-entry to the FBR as stream 65. The recycled hot gas thus serves a dual role as (i) the fluidizing/transport gas for the bubbling bed and (ii) a heat-carrier that redistributes the electrically supplied duty around the SMR loop, while the cyclone-decoupled membrane step enables hydrogen withdrawal without exposing the membrane to solids. Overall, Fig. 5 makes the closure structure explicit: Q-EL/CAT-HEAT/REHEAT account for the electrical heat inputs, CYCL → CAT-HEAT → FBR closes the solids loop, and MEM → SPLIT → CIRC → REHEAT → FBR closes the gas recycle loop with a defined hydrogen product takeoff and recycle ratio.

Catalyst attrition and fines carryover in circulating beds are not modeled in the present process-level Aspen Plus framework. In industrial practice, these are managed by attrition-resistant catalyst/PSD selection, operating within gas-velocity and solids-flux windows that limit erosion, high-efficiency cyclone(s) (and, where needed, secondary capture), and routine catalyst make-up/withdrawal to maintain inventory and activity. The resulting operating consequences (e.g., pressure-drop increase from fines, catalyst loss, downstream fouling/abrasion) are acknowledged as practical design/operating expenditure (OPEX) considerations and are left for future work once a specific reactor/cyclone design is selected.

For the integrated Aspen Plus model, a single consistent thermodynamic property environment was adopted using the Peng–Robinson Boston–Mathias (PR-BM) equation of state, which is widely used for high-temperature $CH_4/H_2/H_2O/CO/CO_2$ syngas systems and has also been used in prior Aspen-based reforming studies Refs. [19,20]. The reforming section was represented at process level using an equilibrium-reactor treatment for benchmarking purposes, consistent with earlier Aspen workflows for membrane-assisted SMR [19,20]. The fluidized-bed catalyst circulation and cyclone were retained at process-architecture level rather than detailed hydrodynamic resolution, because the objective of the present study is integrated plant synthesis rather than reactor-scale hydrodynamic design; this level of abstraction is consistent with prior FBMR/CFFBMR modeling practice [17,19,20,22]. The external Ni membrane was represented as a controlled H_2-selective separator with a specified hydrogen split to the low-pressure permeate, consistent with the lower-cost, lower-permeability nickel-membrane concept discussed in Refs. [15,20]. Electrical heating was modeled explicitly through heat streams and heater blocks, either by specifying outlet temperatures or by specifying duties (Q-EL for reactor-body heating, REHEAT for recycle reheating, and CATHEAT for solids reheating). The preheating train and heat integration were modeled using HEATX blocks with simple design conditions, for example enforcing T_{26}=T_4 (Fig. 2) for the nuclear-heated natural-gas preheater and then further heating the mixed steam-natural-gas stream using an HR-HEAT exchanger driven by SMR effluent with a realistic temperature approach. Design Spec blocks were used to adjust the natural-gas feed to achieve the target H_2 production rate and to adjust steam/makeup water to enforce the selected steam-to-carbon ratio. All reported NET-SMR metrics are plant-gate values; upstream natural-gas supply-chain emissions, electricity-generation mix, nuclear fuel-cycle burdens, and CO_2 transport/storage infrastructure are excluded, consistent with the benchmarking basis adopted in Tables 7 and 8, Refs. [37,38].

6. Results and discussion

The key subsystem for nuclear-SMR integration is the steam Rankine cycle, which makes the link between the nuclear reactor and the steam methane reforming process. The design objective here is to realize a matching of the heat rejection from SMR to the power train of the steam Rankine cycle, while at the same time determining the optimal parameters to provide makeup steam to the steam methane reforming process and to generate power. The main parameters to vary, while seeking to maximize the power generation rate and efficiency are mainly the temperature T_6 at FWH2 exit, the steam HPT extraction rate $\dot{m}_{12}$ to preheat the steam, the discharge pressure of the low-pressure pump P_{19} together with the temperature of water T_{14}, assumed saturated, and the extracted steam flow rate $\dot{m}_{20}$ from LPT.

Under the formulated two-objective optimization from Eq. (13), the pareto frontiers shown in Fig. 6 were obtained. The realization limits of the design are indicated with the filled-dots. The efficiency cannot be further increased above the indicated limits, or otherwise the constraints will not be satisfied, i.e., the pinch point temperature reduces below the minimum, and the extraction steam flow rate may become negative. Also, the curve for $T_6 = 210^{\circ}C$ represents a design limit: under the constraints, the preheat temperature at FWH2 cannot be reduced below that limit.

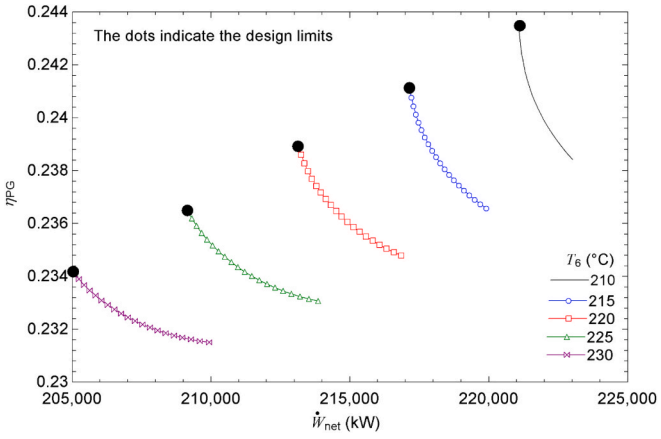

Fig. 6. Pareto frontiers showing power generation efficiency vs net power output.

The influence of steam extraction flow rate from HPT, i.e., $\dot{m}_{12}$, is analyzed separately, with the generated power held constant in a parametric study. In addition, the thermal input from heat recovered from the SMR process is fixed. This study is reported as shown in Fig. 7, which plots the power generation efficiency vs extracted steam flow rate. It is beneficial to extract steam, the flow rate $\dot{m}_{12}$, as this increases the efficiency, but there is a limit to it, as shown in the figure, again, caused by the imposed constraints. Since the thermal power from the nuclear reactor is not fixed for this parametric study, the energy efficiency increases with power generation, as shown. Furthermore, the increase in the extracted steam flow rate is beneficial. The constraints limits determine the maximum possible efficiency and power generation, as well as the best mass flow rate of HPT steam extraction, i.e., $\dot{m}_{12} \approx 24$ kg/s, 222 MW power generation and 24.35% efficiency.

When the power generation efficiency is fixed, the influence of steam extraction from LPT, i.e., $\dot{m}_{20}$ on the generated power $\dot{W}_{net}$ can be observed as shown in Fig. 8. As shown, in these conditions, there is an optimum of steam extraction mass flow rate that maximizes the generated power. It is beneficial to reduce T_{10}, i.e., the water preheating level at FWH2, which will increase the power generation. In addition, the optimum HPT steam extraction rate shifts to the left (lower value) when the power generation increases. The design limit is achieved when $T_{10} = 210^{\circ}$C, for which the optimum $\dot{m}_{20} = 3.563$ kg/s, and power generation is 220 MW.

The parametric and optimization studies conducted so far have helped fix the design parameters of the steam Rankine cycle, which confer the best bridge between the nuclear reactor and the steam methane reforming flowsheet. With this knowledge, the parameters that influence the two-objective optimization of power generation and efficiency are determined, together with their bounds. As such, a two-objective genetic algorithm is used in EES to optimize a multivariable objective function.

The algorithm solves the steam Rankine flowsheet under constraints at each step, while seeking for the maxima. The genetic algorithm is set to 32 individuals, 256 generations, and a 0.2 mutation rate. The pareto algorithm is obtained as shown in Fig. 9. The points of maximum efficiency and maximum power generation are indicated on the figure, at the Pareto frontier. The compromise solution is taken as given in Table 3, which reports all stream parameters at the design point, including the optimized parameters. The compromise maxima for efficiency and power generation are 23.5% and 219 MW, respectively. The duty and entropy generation rate for devices within the steam Rankine cycle flowsheet is given. The entropy generation percentages within the integrated power generation flowsheet are depicted as shown in Fig. 10, with the boiler being most responsible for irreversibility, followed by the high-pressure turbine. Table 4 presents the duty and entropy generation

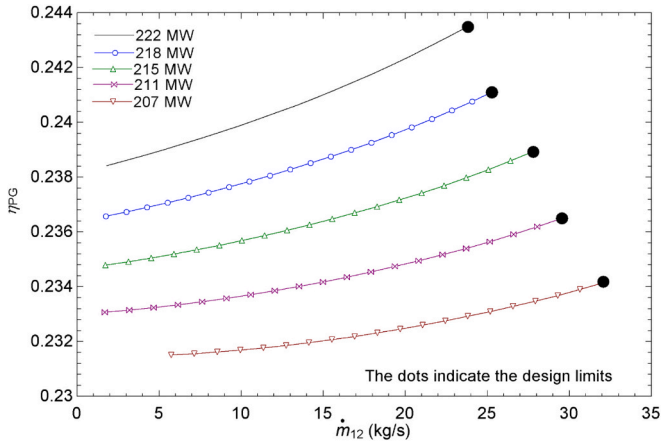

Fig. 7. Rankine cycle efficiency vs steam extraction at HPT for fixed generated power.

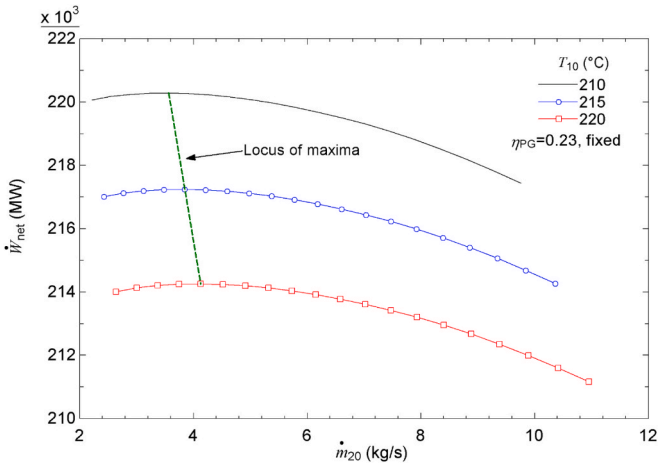

Fig. 8. Power generation vs steam extraction rate from LPT, for fixed efficiency, η_{PG} and several T_{10}.

rate for the devices in the Rankine cycle flowsheet.

An exemplary composition of purified natural gas is assumed to be 97% CH_4, 0.9%C_2H_6, 0.1%C_3H_8, 1%N_2, 1%CO_2, volume percentages. With the preheating train flowsheet is solved in ASPEN Plus and the stream parameters determined as given in Table 5. The input entropy rate in the preheating train is −31.9 kW/K, while the entropy production rate is 15.5 kW/K, the input entropy rate in the reaction train flowsheet is −16.4 kW/K, while the entropy production rate is 15.1 kW/K, the input rate in the separation train flowsheet is −12.1 kW/K and the generation is 10.8 kW/K. Fig. 11 shows the exergy balance of the SMR flowsheets, taken altogether: the exergy efficiency is 85%. The figure summarizes the exergy accounting of the integrated NET-SMR block at the selected design point (Tables 3 and 5). The dominant input is the chemical exergy of natural gas, while the SMNR contributes both high-grade electricity, 45 MW(e), and a smaller direct thermal contribution, 24.4 MW(th), complemented by 34.6 MW(th) of process heat recovery from the SMR/shift/separation cooling duties.

At this operating point, the plant produces 113 t/day of H_2 while generating 614 t/day of concentrated CO_2-rich captured stream at plant gate, corresponding to 9.56 kWh (e)/kg-H_2 of nuclear electricity demand and 6.35 kg-CO_2 captured per kg-H_2. The resulting exergy efficiency of the NET-SMR system is 56%, with remaining losses primarily associated with irreversible reaction/separation/compression steps as reflected by the exergy-destruction segments in Fig. 11. Further, Table 6 gives the design-point performance for NET-SMR.

At the design point, the final concentrated CO_2-rich stream (stream 57) leaves the condensation/separation block at approximately 99.84 wt % CO_2, 0.06 wt% H_2O, and 1.0 wt% NO_2, at about 38.9°C and 1.01 bar. This indicates that the process produces a highly concentrated CO_2-rich stream at plant gate, but not yet a transport/storage-ready CO_2 product. Additional downstream dehydration, impurity polishing (including NO_x cleanup if required), and compression to transport or storage pressure are therefore still required beyond the present condensation/separation block. These downstream CO_2-conditioning loads are not included in the present 13.2 kWh/kg H_2 plant-gate electricity figure, because the current model ends at the concentrated CO_2-rich stream delivered by the condensation/separation block rather than at a fully compressed transport/storage specification.

Unless otherwise stated, the comparative results reported here are expressed on a plant-gate basis; accordingly, the electricity comparison in Table 7 refers to specific onsite electricity demand, whereas the thermodynamic efficiencies reported in Table 6 refer to exergy efficiency on the internal cogeneration accounting basis adopted in this study. Table 7 benchmarks NET-SMR against two realistic refinery alternatives, conventional fired SMR and SMNR-powered PEM

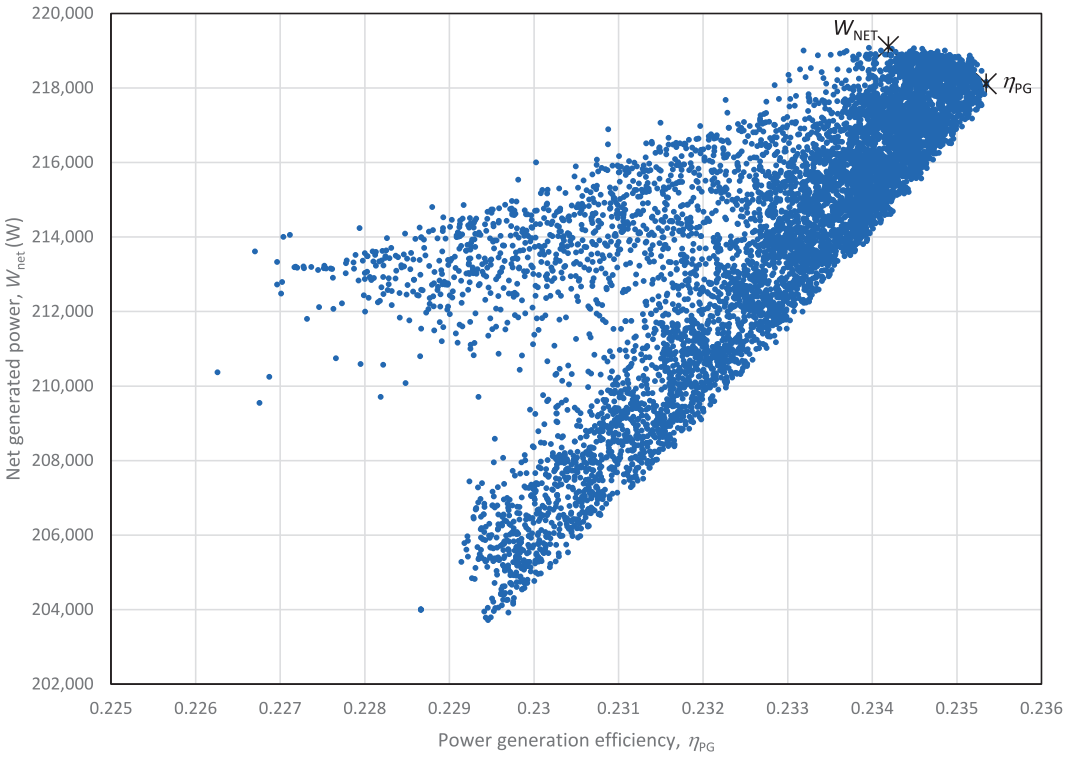

Fig. 9. Two-objective optimization search by genetic algorithm showing the power-efficiency Pareto.

Table 3
Stream parameters of the steam Rankine cycle at design point.

Stream	$\dot{m}$(kg/s)	T °C	P(kPa)	h(kJ/kg)	s(kJ/kg-K)
1	354.6	15,199	343.2	2605	5.298
2	354.6	15,199	543.2	3430	6.492
3	5.963	3344	285.3	2944	6.407
4	5.963	3344	543.2	3551	7.305
5	354.6	15,199	343.2	1618	3.697
6	354.6	15,199	217.9	938	2.475
7	3546	15,199	343.2	1618	3.697
8	3546	15,199	343.2	1717	3.857
9	354.6	15,199	215	937.7	2.506
10	354.6	2106	215	920.5	2.471
11	0.05741	2228	217.9	933.8	2.498
12	0.05741	2228	272.7	2952	6.592
13	0.05741	2106	215	933.8	2.498
14	50.99	303.3	133.9	563	1.676
15	50.99	2106	134.1	565.2	1.676
16	303.6	2106	266.4	2940	6.595
17	45.03	462.8	148.9	2679	6.69
18	45.03	4.247	30	125.7	0.4368
19	45.03	303.3	30.01	126.1	0.4369
20	4.832	303.3	479	3442	8.263
21	45.03	462.8	543.2	3578	8.243
22	40.19	4.247	53.81	2601	8.596
23	50.99	303.3	37.75	158.4	0.5422
24	5.963	303.3	40	167.8	0.5723

electrolysis, to clarify why the nuclear-electrothermal pathway is "electricity-light" at the 113-t/day scale: electrolysis must supply essentially all hydrogen enthalpy electrically, i.e., ~55 kWh/kg H_2 (see Ref. [33]), so for 113 t/day the required electricity is ~6.22 GWh/day, i.e., ~259 MW(e) continuously, whereas NET-SMR meets the same 113 t/day target with 61 MW(e), i.e., 13.2 kWh/kg H_2, because most of the hydrogen energy is still furnished by the chemical exergy of natural gas while electricity provides high-grade heat and auxiliaries. Instead, the NET-SMR is integrated with a nuclear reactor that delivers 926 MW(th) at the primary loop, while the Rankine cycle produces 235 MW(e), i.e., 24 MW(e) less than what an equivalent proton exchange membrane electrolyzer (PEME) would require. In addition, besides generating the hydrogen, NET-SMR is able to generate more profit from exporting 173 MW(e) to local users, while also capturing 614 t/CO_2 which is eligible to tax credit and clean energy incentives. All metrics in Table 7 are plant-gate (onsite) values; upstream natural-gas supply-chain emissions (methane leakage), electricity-generation mix, nuclear fuel cycle, and CO_2 transport/storage infrastructure are excluded.

As summarized in Table 7, the NET-SMR design can be described in terms of the major process equipment and the practical scale-up implications. The electrified SMR core is implemented as a circulating fluidized-bed reformer rated at 35 MW, operating at ~30 atm and 700°C, with an indicative vessel size of ~3 m in diameter × 12 m in height. Reforming heat is supplied by direct electrical energization, represented here by ~80 tubular heating elements, each approximately 0.10 m in diameter × 12 m in length, arranged to deliver uniform, high-grade heat to the circulating catalyst/solids loop. Those deliver 12 MW inside the SMR reactor vessel. The circulating fluidized bed allows the dense catalyst flow to be reheated in the downcomer, with a design duty of 5.5 MW provided at the wall on a tall section. The catalysts is heated into four diplegs of 0.5 m diameter that return the separated catalyst through downcomers of 4 cyclones, each duct heated at 90 kW/m^2 at the wall, such that the catalyst is heated from 700°C to 800°C before being reinjected into the reaction zone: duty of each heater is 1.375 MW. The recirculated gas as is reheated in 4 electrical heaters of 3.625 MW. Two shift stages provide downstream equilibrium conditioning: a high-temperature WGS reactor around 22 atm rejecting ~2.3 MW (tube–-shell form, ~1.5 m shell diameter × 7 m length) with an indicative catalyst inventory of ~6 t of Fe_2O_3/Cr_2O_3, followed by a low-temperature WGS reactor near 20 atm rejecting ~2.4 MW (about 1.5 m diameter × 8 m length) using a Cu–Zn–Al oxide catalyst to complete CO cleanup and boost hydrogen yield. Two hydrogen-selective Ni-based membrane are sized, supported ultrathin Ni alloy film of 5 μm: 1) to generate stream 29 a membrane of ~3200 m^2, positioned to withdraw H_2 in situ and thereby shift equilibrium so that deep conversion is achieved at the reduced reforming temperature target at the electrified

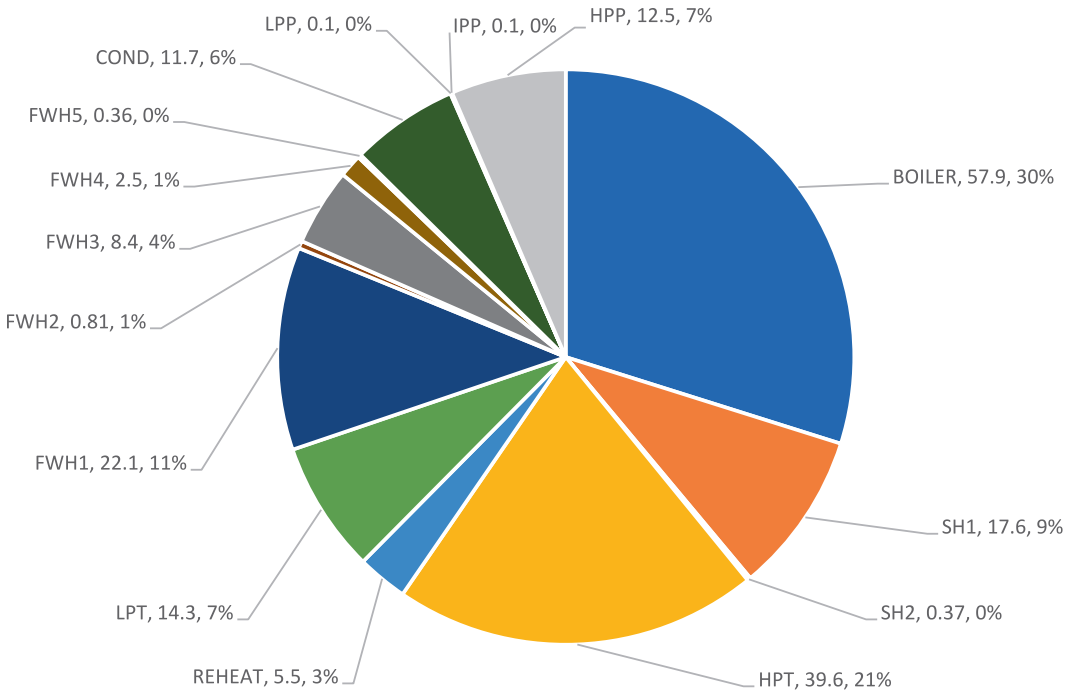

Fig. 10. Entropy generation percentages within the integrated power generation flowsheet.

Table 4
Thermal/power duty and entropy generation rate for steam Rankine flowsheet devices.

DEVICE	BOILER	SH1	SH2	HPT	REHEAT	LPT	FWH1	FWH2	FWH3	FWH4	FWH5	COND	LPP	IPP	HPP
$\dot{E}$, MW	350	292	3.6	185	40.5	39.9	241	Adiab.	2.36	4.0	1.40	5.32	0.015	0.11	6.1
$\dot{S}_g$, kW/K	57.9	17.6	0.37	39.6	5.5	14.3	22.1	0.81	8.4	2.5	0.36	11.7	0.1	0.1	12.5

Here, $\dot{S}_g$ is entropy generation rate, $\dot{E}$ refers to heat duty $\dot{Q}$ or power $\dot{W}$ whichever applies. For feedwater heaters, external coil duty is given.
Total $\dot{S}_g = 193.8$ kW/K, $\dot{S}_{in} = 1417$ kW/K. FWH1 is supplied by 25.5 MW from heat recovery and 215.5 MW by nuclear heat.

SMR reactor, and 2) to generate stream 36, a 670 m^2 separation membrane to extract hydrogen from product gas. Auxiliary power and pressure management related to membrane operation are handled by a three-stage compression station with two intercoolers, requiring 2.4 MW electric power and rejecting ~1.66 MW(th) of intercooling duty.

For CO_2 handling and energy recovery, the tail-gas oxidation/capture block is represented by a compact high-pressure combustor operating near 25 atm with an adiabatic flame temperature of 1442°C; an indicative geometry is ~1 m diameter × 2 m length, and the volumetric heat-release intensity is taken as ~40 MW(th) per m^3 (order-of-magnitude sizing). The hot products expand through a small gas turbine with TIT 1010°C, expanding approximately from 25 atm to 3 atm; a representative machine description is a ~700 mm rotor, ~2 m rotor length, ~5 stages, within a package envelope of roughly 2.5 m diameter × 6 m and 6.5 MW power output. This block provides a compact route to recover part of the residual chemical energy while preserving a concentrated CO_2 stream for downstream dehydration/conditioning.

These equipment-level figures support the chief conclusion drawn from Table 7: SMNR-assisted electrified SMR is a promising and, in principle, technologically ready pathway for large refinery hydrogen, because the membrane-assisted reformer can lower the required reforming temperature while the electric heater decouples reactor choice from process temperature, making the concept compatible with a broad range of near-future SMNRs. The capacity logic is also favorable: SMR technology is already proven at industrial scale (often 1000 + t H_2/day), whereas the largest single electrolysis plants are still typically ~100 t/day class, so using SMNR electricity to "electrify SMR heat" preserves the established large-unit process architecture while enabling high CO_2 capture in the syngas loop rather than dealing with dilute furnace flue gas. Cost and plant architecture point in the same direction: electrolysis remains more capital-intensive at roughly $1–1.8 k per (kg-$H_2$/day) compared with SMR-class systems at $0.5–0.9 k per (kg-$H_2$/day), and electrolysis is inherently more distributed (i.e. thousands of repeating cells, many stacks, extensive manifolding, and more small parts (cells, seals, small pipes) requiring precise alignment) while SMR is comparatively centralized, dominated by fewer but larger units (reformer and shift vessels) that naturally scale to high throughput; in addition, PEM membranes typically require costly replacement on the order of ~5 years, which adds recurring OPEX and outage planning considerations.

The scale-driven complexity difference can be illustrated by the 113 t/day benchmarking basis used in Table 7. If one takes the alkaline electrolyzer option sized to 113 t/day, this can be represented by about 10,500 cells of 4 m^2 each, arranged as ~375 cells per stack, i.e., ~28 stacks in parallel, with an indicative piping inventory on the order of 2.6 km (for example, ~2028 m of stack-level piping plus ~507 m of headers and ~101 m of cross-connects, with typical line sizes around 4-inch for water supply and 2-inch for product gas). If one takes the PEM electrolyzer option at the same output, this can be represented by about 8867 cells of 1 m^2 each, arranged as ~80 cells per stack, i.e., ~111 stacks in parallel, with a still substantial but lower indicative piping inventory of ~1.1 km (e.g., ~708 m per-stack piping, ~120 m headers, ~200 m flow distribution, and ~64 m redundancy). These counts and lengths are not "minor details": they reflect the fundamental reason

Table 5
Stream parameters within the SMR flowsheets, at design point.

Stream	Composition (% wt)	$\dot{m}$(kg/s)	T(°C)	P(bar)	h(kJ/kg)	s(kJ/kg-K)
25	93.8CH_4, 1.6C_2H_6, 0.26C_3H_8, 1.69 N_2, 2.65CO_2	2.67	25.0	33.4	−4679	−6.57
26	93.8CH_4, 1.6C_2H_6, 0.26C_3H_8, 1.69 N_2, 2.65CO_2	2.67	543.0	32.4	−3084	−3.59
27	71·.7H_2O, 26.5CH_4, 0.46C_2H_6, 0.07C_3H_8, 0.48 N_2, 0.79CO_2	9.44	541.8	32.4	−9781	−2.24
28	71·.7H_2O, 26.5CH_4, 0.46C_2H_6, 0.07C_3H_8, 0.48 N_2, 0.79CO_2	9.44	700.0	31.4	−9338	−1.73
29	100H_2(G)	0.786	701.3	1.013	9874	17.2
30	47·.6H_2O, 2.89CH_4, 0.5 N_2, 2.5CO_2, 1.0H_2, 45.51CO	8.66	700.0	30.4	−7362	1.21
31	47·.6H_2O, 2.89CH_4, 0.5 N_2, 2.5CO_2, 1.0H_2, 45.51CO	8.66	350.0	29.4	−8017	0.39
32	32·.8H_2O, 2.89CH_4, 0.5 N_2, 38.3CO_2, 2.64H_2, 22.87CO	8.66	350.0	27.4	−8324	0.27
33	32·.8H_2O, 2.89CH_4, 0.5 N_2, 38.3CO_2, 2.64H_2, 22.87CO	8.66	250.0	26.4	−8707	−0.03
34	18·.3H_2O, 2.9CH_4, 0.5 N_2, 74.0CO_2, 4.3H_2	8.66	250.0	25.4	−8822	−0.43
35	18·.3H_2O, 2.9CH_4, 0.5 N_2, 74.0CO_2, 4.3H_2	8.66	584.1	25.2	−8168	0.53
36	18·.3H_2O, 2.9CH_4, 0.5 N_2, 74.0CO_2, 4.3H_2	8.66	652.6	25.0	−8026	0.69
37	100H_2(G)	0.37	653.8	1.013	9165	16.5
38	19·.1H_2O, 3.0CH_4, 0.5 N_2, 77.3CO_2	8.29	625.6	25.0	−8798	0.28
39	100H_2(G)	1.16	686.2	1.013	9647	17.0
40	100H_2(G)	1.16	615.0	1.013	8590	15.9
41	100H_2(G)	1.16	250.0	1.013	3256	8.13
42	100H_2(G)	1.16	160.0	1.013	1948	5.38
43	100H_2(G)	1.16	30.0	1.013	71.8	0.24
44	100H_2(G)	1.16	60.0	25.3	514.2	−11.7
45	100H_2O(L)	1.24	25.0	30.0	−16,031	−9.06
46	100H_2(G)	0.14	60.0	25.3	514.2	−11.7
47	O_2(G)	1.10	60.0	25.3	27.1	−0.74
48	22·.9H_2O, 75.5CO_2, 1.6NO_2	9.39	1442.5	25.3	−7766	1.22
49	22·.9H_2O, 75.5CO_2, 1.6NO_2	9.39	1009.8	3.04	−8469	1.28
50	22·.9H_2O, 75.5CO_2, 1.6NO_2	9.39	730.2	3.0	−8895	0.91
51	22·.9H_2O, 75.5CO_2, 1.6NO_2	9.39	250.0	2.96	−9553	0.02
52	22·.9H_2O, 75.5CO_2, 1.6NO_2	9.39	160.0	2.93	−9662	−0.11
53	22·.9H_2O, 75.5CO_2, 1.6NO_2	9.39	40.0	2.91	−10,362	−1.98
54	99·.5H_2O, 0.03CO_2, 0.47NO_2	2.07	40.0	2.04	−15,880	−8.82
55	1·.2H_2O, 96.9CO_2, 1.9NO_2	7.32	40.0	2.04	−8802	−0.04
56	39·.6H_2O, 60.4NO_2	0.22	38.9	1.01	−5843	−4.34
57	99.84CO_2, 0·.06H_2O, 1.0NO_2	7.10	38.9	1.01	−8924	0.10
58	100H_2(G)	1.40	60.0	25.3	514.2	−11.7
59	26·.6H_2O, 1.6CH_4, 0.3 N_2, 1.4CO_2, 5.6H_2, 25.5CO, 5.8Ni, 33.2Al_2O_3	77.3	700.2	30.4	−8727	0.58
60	0.15Ni, 0.85Al_2O_3	30.1	700.0	30.4	−13,131	−1.27
61	43·.6H_2O, 2.3CH_4, 0.5 N_2, 2.3CO_2, 9.2H_2, 42.1CO	47.2	700.0	30.4	−5924	1.75
62	47·.6H_2O, 2.89CH_4, 0.5 N_2, 2.5CO_2, 1.0H_2, 45.51CO	42.9	700.0	30.4	−7362	1.21
63	47·.6H_2O, 2.89CH_4, 0.5 N_2, 2.5CO_2, 1.0H_2, 45.51CO	42.1	700.0	30.4	−7362	1.21
64	47·.6H_2O, 2.89CH_4, 0.5 N_2, 2.5CO_2, 1.0H_2, 45.51CO	42.1	717.4	32.4	−6142	1.69
65	47·.6H_2O, 2.89CH_4, 0.5 N_2, 2.5CO_2, 1.0H_2, 45.51CO	42.1	900.0	32.4	−7165	1.38
66	0.15Ni, 0.85Al_2O_3	30.1	800.0	30.4	−12,946	−1.09

electrolysis plants tend to become mechanically and electrically complex at >100 t/day, because capacity is achieved by multiplication of many small, precision components, whereas NET-SMR achieves the same throughput by scaling a small number of larger pressure vessels and heat/mass-transfer devices. Finally, from a first-principles energy standpoint, the comparison remains structurally robust: splitting water requires roughly an order of magnitude more energy per unit hydrogen than liberating hydrogen from natural gas, so even with low-carbon electricity, the all-electrolysis route carries a much larger electricity footprint at refinery scale than an electro-thermal SMR architecture that uses electricity mainly as high-grade heat and for auxiliaries.

To position NET-SMR against the most relevant low-carbon industrial hydrogen options, Table 8 compares the present design with literature benchmarks for the two principal blue-hydrogen pathways, SMR + CCS and ATR + CCS. NET-SMR values are direct outputs of the present plant-gate model, whereas the comparator values are taken from the cited benchmark literature on the closest comparable system boundary. Accordingly, the table should be interpreted as an indicative positioning exercise rather than a fully harmonized cradle-to-gate techno-economic or lifecycle assessment.

Table 8 positions NET-SMR relative to the two principal blue-hydrogen pathways, SMR + CCS and ATR + CCS, using three

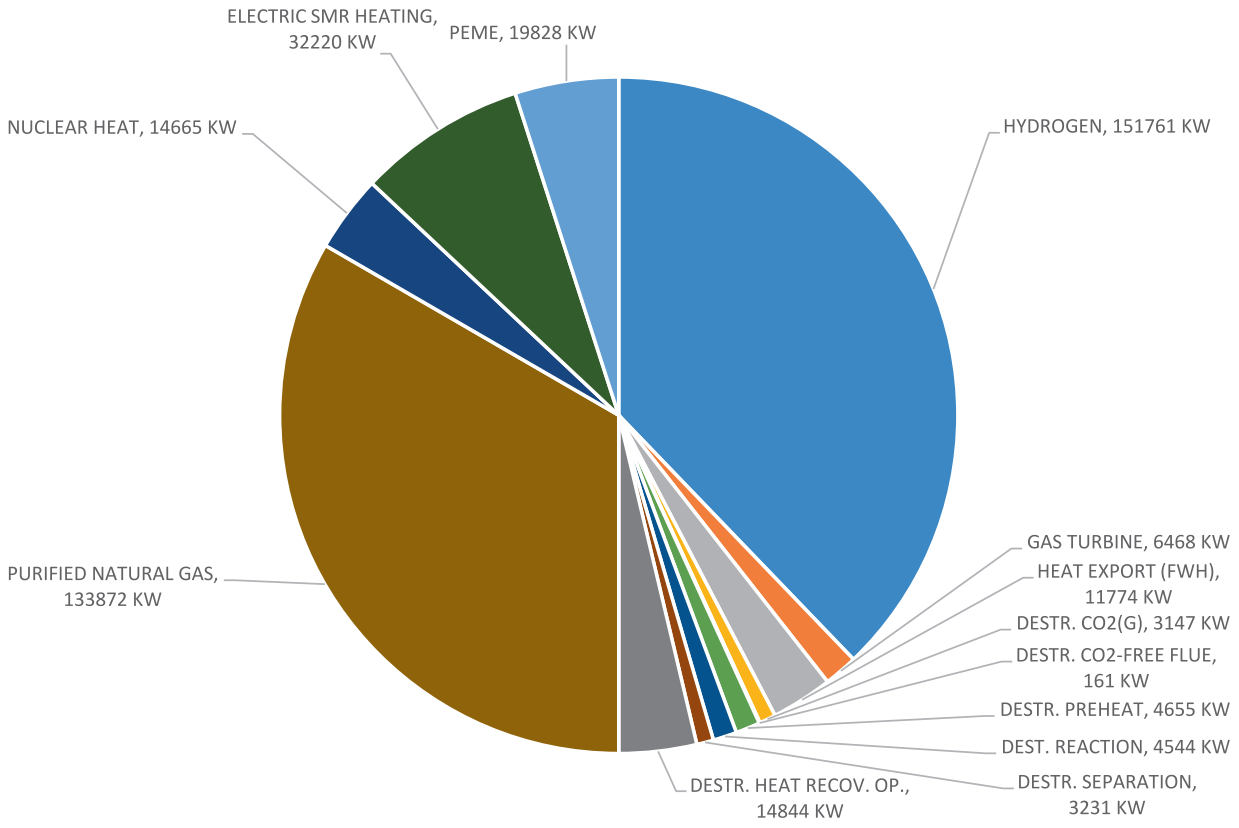

Fig. 11. Exergy balance chart on the steam methane reforming process.

Table 6
NET-SMR design-point performance metrics (plant-level).

Category	Metric	Value	Normalized (per kg H_2)
Product	Hydrogen production	113 t/day	1.00
Capture	CO_2 captured	614 t/day	5.43 kg/kg H_2
Feed	Natural gas consumption	231 t/day	2.04 kg/kg H_2
Water	Net water consumption	513 t/day	4.54 kg/kg H_2
Nuclear inputs	SMNR heat supplied to SMR process	24.4 MW (th)	3.1 kWh(th)/kg H_2
	SMNR heat supplied to Rankine cycle	902 MW (th)	192 kWh(th)/kg H_2
	Total SMNR heat supplied to NET-SMR	926 MW (th)	197 kWh(th)/kg H_2
	Exergy of nuclear heat input	648 MW (e)	138 kWh(th)/kg H_2
Integration	Electrical power to SMR reactor	32.2 MW (e)	6.85 kWh(e)/kg H_2
	Electrical power to PEME	19.8 MW (e)	4.21 kWh(e)/kg H_2
	Power to H_2 compressors	9.91 MW (e)	2.11 kWh(e)/kg H_2
Recovery	Net power from energy recovery	6.47 MW (e)	1.38 kWh(e)/kg H_2
	Heat recovered from SMR loops	34.6 MW (th)	7.4 kWh(th)/kg H_2
Exergy	SMR-only exergy efficiency	85%	–
	Total Rankine power output	235 MW (e)	50 kWh/kg H_2
	Hydrogen product exergy	152 MW	32 kWh/kg H_2
	Net output power	173 MW (e)	37 kWh/kg H_2
	Overall exergy efficiency	56%	–

Note: Exergy efficiencies in Table 6 are reported on the internal plant-gate hydrogen-plus-power cogeneration accounting basis adopted in this study; they are not intended as full primary-energy or lifecycle efficiency metrics.

Table 7
Benchmark comparison at ~100 t/day scale (indicative).

Table Metric	Conventional SMR (fired)	NET-SMR (this work)	SMNR-PEM electrolysis
H_2 production	113 t/day	113 t/day	113 t/day (target)
Direct CO_2 emissions	~9–12 kg/kg H_2	~0 (direct CO_2 capture applied)	~0 direct
Electricity use	low–moderate (aux.)	13.2 kWh/kg H_2	~55 kWh/kg H_2
Required electric power	–	61 MW(e) (*)	~259 MW(e)
CO_2 captured	none / optional CCS	614 t/day	none
CAPEX intensity (order of mag.)	0.5–0.9 k$/(kg-$H_2$/day)	similar class as SMR	~1.8 k$/(kg-$H_2$/day)

(*) including hydrogen compression.

Table 8
Comparison of NET-SMR to blue hydrogen pathways.

Technology	NET-SMR	Blue hydrogen, Refs. [37,38]	
		SMR + CCS	ATR + CCS
Specific electricity demand, kWh/kg H_2	13.2	2.04	4.00
Direct plant CO_2 emissions, kg CO_2/kg H_2	Zero*	0.38	0.51
CAPEX intensity (order of mag.), k$/(kg-$H_2$/day)	0.5–0.9	1.7	1.4

* direct CO_2 capture applied.

indicators already emphasized in this paper: specific electricity demand, direct plant CO_2 emissions, and order-of-magnitude CAPEX intensity. NET-SMR requires 13.2 kWh/kg H_2 and, on the stated plant-gate basis,

reports zero direct plant CO_2 emissions because direct CO_2 capture is applied. The corresponding NETL benchmark values are 2.04 kWh/kg H_2 and 0.38 kg CO_2/kg H_2 for SMR + CCS, and 4.00 kWh/kg H_2 and 0.51 kg CO_2/kg H_2 for ATR + CCS. For capital intensity, the blue-hydrogen benchmarks report TOC values of 1.735 and 1.372 k$/(kg-$H_2$/day), reported here in rounded form as 1.7 and 1.4 k$/(kg-$H_2$/day).

For additional cost context, literature benchmarks report indicative levelized hydrogen costs of about 1.64 $/kg H_2 for SMR + CCS and about 1.59 $/kg H_2 for ATR + CCS, Ref. [37,38]. Current PEM electrolysis remains substantially more expensive, typically on the order of about 5–7 $/kg H_2 depending on electricity source, capacity factor, and installed capital cost, Ref. [33]. A fully harmonized LCOH for NET-SMR is beyond the direct scope of the present steady-state plant-gate model, because it would require explicit assumptions for electricity and natural-gas prices, financing, carbon policy, SMNR cost allocation, and CO_2 transport/storage charges. The present discussion should therefore be read as an indicative parametric cost comparison rather than a full techno-economic assessment.

7. Conclusion

This paper develops and assesses a nuclear electro-thermal steam-methane reforming (NET-SMR) architecture for refinery-scale hydrogen production in which a small modular nuclear reactor (SMNR) supplies steady steam and electricity, while the endothermic reforming duty is delivered electrically to a compact circulating fluidized-bed reformer (CFBR) with cyclone-decoupled external separation. The central design choice – electrifying the reforming heat rather than the chemistry itself – preserves the scale advantages and process familiarity of SMR while confining carbon to concentrated process streams compatible with high-rate capture.

At the modeled design point, the integrated Aspen Plus + EES Rankine-cycle synthesis shows that NET-SMR can deliver 113 t/day H_2 while producing 614 t/day of concentrated CO_2-rich captured stream at plant gate, with a total electricity demand of 13.2 kWh/kg H_2 including auxiliaries and compression, compared with about 55 kWh/kg H_2 for SMNR-powered PEM electrolysis at the same hydrogen output. This "electricity-light" characteristic is structural: most of the hydrogen enthalpy is provided by the chemical exergy of natural gas, while electricity is used primarily to supply high-grade heat and drive separation and compression. On the chosen plant-gate cogeneration accounting basis, the NET-SMR block achieves an SMR-only exergy efficiency of about 85% and an overall integrated exergy efficiency of about 56%.

These results support three main conclusions. First, NET-SMR provides a credible route to deep decarbonization of refinery hydrogen without requiring the very large electrical supply implied by all-electrolysis at scales above 100 t/day. Second, the proposed architecture is reactor-neutral: it can be coupled to a range of SMNR types because electrical heating decouples reformer temperature control from reactor outlet temperature, while nuclear steam and power support robust cogeneration. Third, the equipment count and scaling logic remain SMR-like, with a small number of large process units rather than many thousands of repeating electrolysis cells, suggesting an integration pathway that is closer to existing refinery practice.

The present work is deliberately an integrated, steady-state synthesis, and the next stage should focus on detailed CFBR hydrodynamics and cyclone/dipleg operability, membrane durability and pressure-drop behavior under realistic conditions, dynamic load-following and control, and full site-specific techno-economic assessment. Addressing these items will tighten the engineering feasibility envelope and clarify where NET-SMR is most competitive relative to conventional SMR + CCS and SMNR-electrolysis. Because CO_2 is captured as a concentrated stream, the configuration may also offer access, depending on jurisdiction, to carbon-credit, carbon-tax, or clean-energy incentive frameworks that could help offset initial capital cost.

CRediT authorship contribution statement

Rami S. El-Emam: Writing – review & editing, Writing – original draft, Supervision, Project administration, Methodology, Formal analysis, Conceptualization. **Rahaf Ajaj:** Writing – review & editing, Supervision, Project administration, Conceptualization. **Khaoula Khlie:** Supervision, Project administration. **Calin Zamfirescu:** Writing – original draft, Visualization, Supervision, Project administration, Methodology, Investigation, Formal analysis, Conceptualization.

Declaration of competing interest

The authors declare that they have no known competing financial interests or personal relationships that could have appeared to influence the work reported in this paper.

Data availability

Data will be made available on request.

References

[1] Karibe H, Sair S, Faik A, Ait Ousaleh H. Electrified steam methane reforming: a review of heating technologies, challenges, and prospects. Int J Hydrogen Energy 2025;133:200–13.

[2] Song H, Liu Y, Bian H, Shen M, Lin X. Production method by electrified steam methane reforming with renewable energy accommodation. Energ Conver Manage 2022;258:115513.

[3] Alminda MR, Vendelbob SB, Hansenc MF, Vinumd MG, Frandsena C, Mortensene PM, et al. Improving performance of induction-heated steam methane reforming. Catal Today 2020;342:13–20.

[4] Vinum MG, Almind MR, Engbaek JS, Vendelbo SB, Hansen MF, Frandsen C, et al. Dual-function cobalt–nickel nanoparticles tailored for high-temperature induction-heated steam methane reforming. Angew Chem Int Ed Engl 2018;57:10569–73.

[5] From TN, Partoon B, Rautenbach M, Østberg M, Bentien A, Aasberg-Petersen K, et al. Electrified steam methane reforming of biogas for sustainable syngas manufacturing and next-generation of plant design: a pilot plant study. Chem Eng J 2024;479:147205.

[6] Wismann ST, Engbæk JS, Vendelbo SB, Bendixen FB, Eriksen WL, Aasberg-Petersen K, et al. Electrified methane reforming: a compact approach to greener industrial hydrogen production. Science 2019;364(6442):756–9.

[7] Wismann, S. T. (2019). Electrically heated steam methane reforming [Doctoral dissertation, Technical University of Denmark].

[8] Topsoe, eREACT® Hydrogen: The future of blue hydrogen. Available at: https://www.topsoe.com/our-resources/knowledge/our-products/equipment/ereact-hydrogen.

[9] Cui X, Çıtmacı B, Peters D, Abdullah F, Wang Y, Hsu E, et al. Estimation-based model predictive control of an electrically-heated steam methane reforming process. Digital Chem Eng 2024;11:100153.

[10] Çıtmacı B, Peters D, Cui X, Abdullah F, Almunaifi A, Chheda P, et al. Feedback control of an experimental electrically-heated steam methane reformer. Chem Eng Res Des 2024;206:469–88.

[11] Çıtmacı B, Cui X, Abdullah F, Richard D, Peters D, Wang Y, et al. Model predictive control of an electrically-heated steam methane reformer. Digital Chem Eng 2024;10:100138.

[12] Rossi, Mosè and Fanti, Obdulio and Pacca, Sérgio Almeida and Mancinelli, Enrico and Comodi, Gabriele, E-Reformer for Sustainable Hydrogen Production: Enhancing Efficiency in the Steam Methane Reforming Process. Available at SSRN: https://ssrn.com/abstract=5225660 or https://doi.org/10.2139/ssrn.5225660.

[13] Bukkholm IS. Electric steam methane reforming: Economical and environmental implications of replacing methane with electricity for heating in a steam methane reformer (Master's thesis, Norwegian University of Science and Technology, Faculty of Natural Sciences, Department of Energy and Process Engineering). 2021.

[14] Roses L, Gallucci F, Manzolini G, van Sint Annaland M. Experimental study of steam methane reforming in a Pd-based fluidized bed membrane reactor. Chem Eng J 2013;222:307–20.

[15] Adris A-EM. A fluidized bed membrane reactor for steam methane reforming (Doctoral dissertation). University of British Columbia, Vancouver, Canada. 1994.

[16] Patil CS, van Sint Annaland M, Kuipers JAM. Fluidised bed membrane reactor for ultrapure hydrogen production via methane steam reforming: experimental demonstration and model validation. Chem Eng Sci 2007;62:2989–3007.

[17] Abashar MEE, Alhumazi KI, Adris AM. Investigation of methane-steam reforming in fluidized bed membrane reactors. Trans Instit Chem Eng, Part A 2003;81:251–8.

[18] Shahkarami P, Fatemi S. Mathematical modeling and optimization of combined steam and dry reforming of methane process in catalytic fluidized bed membrane reactor. Chem Eng Commun 2015;202:774–86.

[19] Ye G, Xie D, Qiao W, Grace JR, Lim CJ. Modeling of fluidized bed membrane reactors for hydrogen production from steam methane reforming with Aspen Plus. Int J Hydrogen Energy 2009;34(18):4755–62.

[20] Pasha MK, Ahmad I, Mustafa J, Kano M. Modeling of a nickel-based fluidized bed membrane reactor for steam methane reforming process. J Chem Soc Pak 2019;41(2):219.
[21] Chen Z, Yan Y, Elnashaie SSEH. Novel circulating fast fluidized-bed membrane reformer for efficient production of hydrogen from steam reforming of methane. Chem Eng Sci 2003;58(20):4335–49.
[22] Adris AM, Lim CJ, Grace JR. The fluidized-bed membrane reactor for steam methane reforming: model verification and parametric study. Chem Eng Sci 1997;52(10):1609–22.
[23] Reyes Molina E. A., Sweeney K. P., Root S. J., Guaita N., Cheng W.-C., Joseck F. C., Knighton L. T., Boardman R. D. 2024. Technical and economic assessment and gap analysis of advanced nuclear reactor integration with a reference oil refinery (Report No. INL RPT-24-78634). Idaho National Laboratory.
[24] Novotny V., Sweeney K. P., Worsham E. K., Reyes Molina E. A., Root S. J., Joseck F., Choi B.-H., Popli N., Kim J., Knighton T., & Saeed R. M. 2024. Thermal integration of advanced nuclear reactors with a reference refinery, methanol synthesis, and a wood pulp plant (Report No. INL/RPT-24-76435). Idaho National Laboratory.
[25] Rieks M, Bellinghausen R, Kockmann N, Mleczko L. Experimental study of methane dry reforming in an electrically heated reactor. Int J Hydrogen Energy 2015;40(42):15940–51.
[26] Wang Y, Chen W, Zhang L, Zhao X, Gao Y, Dinavahi V. Small modular reactors: an overview of modeling, control, simulation, and applications. IEEE Access 2024;12:39628.
[27] Wu C, Wu B, Zhang H, Yin H. Study on the performance of membrane reactor using steam methane reforming for hydrogen production heated by HTGR. Nucl Eng Technol 2025;57:103744.
[28] Hori M, Matsui K, Tashimo M, Yasuda I. Synergistic hydrogen production by nuclear-heated steam reforming of fossil fuels. Prog Nucl Energy 2005;47(1–4):519–26.
[29] Hoseinzade L, Adams II TA. Modeling and simulation of an integrated steam reforming and nuclear heat system. Int J Hydrogen Energy 2017;42(48):25048–62.
[30] Schröders S, Verfondern K, Allelein H-J. Energy economic evaluation of solar and nuclear driven steam methane reforming processes. Nucl Eng Des 2018;329:234–46.
[31] Song H, Bian H, Lin X, Liu Y. Storage and regeneration of renewable energy via hydrogen - a novel power system integrating electrified methane reforming and gas-steam combined cycle. Int J Hydrogen Energy 2024;95:118–28.
[32] Klein, S.A., 2018. Engineering Equation Solver Manual. F-Chart Software, Madison, WI. Available at: https://www.fchart.com/assets/downloads/ees_manual.pdf.
[33] Hubert M, Peterson D, Miller E, Vickers J, Mow R, Howe C. 2024. Clean Hydrogen Production Cost Scenarios with PEM Electrolyzer Technology (DOE Hydrogen Program Record 24005, May 20, 2024). U.S. Department of Energy, Hydrogen and Fuel Cell Technologies Office. Available at: https://www.hydrogen.energy.gov/docs/hydrogenprogramlibraries/pdfs/24005-clean-hydrogen-production-cost-pem-electrolyzer.pdf.
[34] Ryan L. Hydrogen Production: Overview and Issues for Congress (CRS Report R48196, Oct 3, 2024). Congressional Research Service. 2024. Available at: https://www.congress.gov/crs-product/R48196.
[35] European Hydrogen Observatory (Clean Hydrogen Partnership). Cost of hydrogen production (levelised cost by technology and country; reference years 2022–2024). Accessed February 2026. Available at: https://observatory.clean-hydrogen.europa.eu/index.php/hydrogen-landscape/production-trade-and-cost/cost-hydrogen-production.
[36] Patel GH, Havukainen J, Horttanainen M, Soukka R, Tuomaala M. Climate change performance of hydrogen production based on life cycle assessment. Green Chem 2024;26:992–1006. https://doi.org/10.1039/D3GC02410E.
[37] S. McNaul, C. White, R. Wallace, T. Warner, H. S. Matthews, J. Ma, M. Ramezan, E. Lewis, "Hydrogen Shot Technology Assessment: Thermal Conversion Approaches," National Energy Technology Laboratory, Pittsburgh, December 5, 2023.
[38] E. Lewis, S. McNaul, M. Jamieson, M.S. Henriksen, H.S. Matthews, J. White, L. Walsh, J. Grove, T. Shultz, T.J. Skone, R. Stevens, Comparison of Commercial, State-of-the-Art, Fossil-Based Hydrogen Production Technologies, U.S. Department of Energy, National Energy Technology Laboratory (NETL), DOE/NETL-2022/3241, April 12, 2022.